Pseudomonas fluorescens MFE01 delivers a putative type VI secretion amidase that confers biocontrol against the soft-rot pathogen Pectobacterium atrosepticum

Yvann Bourigault, Charly A Dupont, Jonas B Desjardins, Thierry Doan, Mathilde Bouteiller, Hugo Le Guenno, Sylvie Chevalier, Corinne Barbey, Xavier Latour, Eric Cascales, et al.

Received: 14 December 2022 | Accepted: 15 August 2023

DOI: 10.1111/1462-2920.16492

RESEARCH ARTICLE

ENVIRONMENTAL MICROBIOLOGY Applied Microbiology International

Pseudomonas fluorescens MFE01 delivers a putative type VI secretion amidase that confers biocontrol against the soft-rot pathogen *Pectobacterium atrosepticum*

Yvann Bourigault[1,2] | **Charly A. Dupont**[1,2] | **Jonas B. Desjardins**[3] | **Thierry Doan**[3] | **Mathilde Bouteiller**[1,2] | **Hugo Le Guenno**[4] | **Sylvie Chevalier**[1] | **Corinne Barbey**[1,2] | **Xavier Latour**[1,2] | **Eric Cascales**[3] | **Annabelle Merieau**[1,2]

[1]Laboratoire de Communication Bactérienne et Stratégies Anti-infectieuses (CBSA, UR 4312), Univ Rouen Normandie, Université Caen Normandie, Normandie Univ, Rouen, France

[2]Structure Fédérative de Recherche Normandie Végétale, NORVEGE Fed4277, Mont-Saint-Aignan, France

[3]Laboratoire d'Ingénierie des Systèmes Macromoléculaires (LISM, UMR 7255), Institut de Microbiologie de la Méditerranée (IMM, FR3479), CNRS—Aix-Marseille Univ, Marseille, France

[4]Plateforme de Microscopie, Institut de Microbiologie de la Méditerranée (IMM, FR3479), CNRS—Aix-Marseille Univ, Marseille, France

Correspondence
Eric Cascales, Laboratoire d'Ingénierie des Systèmes Macromoléculaires (LISM, UMR 7255), Institut de Microbiologie de la Méditerranée, CNRS—Aix-Marseille Univ, Marseille, France.
Email: cascales@imm.cnrs.fr

Annabelle Merieau, Laboratoire de Communication Bactérienne et Stratégies Anti-infectieuses (CBSA, UR 4312), Univ Rouen Normandie, Université Caen Normandie, Normandie Univ, F-76000 Rouen, France.
Email: annabelle.merieau@univ-rouen.fr

Funding information
Structure Fédérative de Recherche Normandie Végétal NORVEGE Fed4277; Ministère de l'Enseignement Supérieur; de la Recherche et de l'Innovation; Régions Bretagne; Normandie & Pays de Loire; Evreux Portes de Normandie agglomeration; Pôle de Compétitivité Valorial; CNRS; Aix-Marseille Université; Fondation pour la Recherche Médicale, Grant/Award Numbers: ECO202206015565, DEQ20180339165; Fondation Bettencourt-Schueller

Abstract

The type VI secretion system (T6SS) is a contractile nanomachine widespread in Gram-negative bacteria. The T6SS injects effectors into target cells including eukaryotic hosts and competitor microbial cells and thus participates in pathogenesis and intermicrobial competition. *Pseudomonas fluorescens* MFE01 possesses a single T6SS gene cluster that confers biocontrol properties by protecting potato tubers against the phytopathogen *Pectobacterium atrosepticum* (Pca). Here, we demonstrate that a functional T6SS is essential to protect potato tuber by reducing the pectobacteria population. Fluorescence microscopy experiments showed that MFE01 displays an aggressive behaviour with an offensive T6SS characterized by continuous and intense T6SS firing activity. Interestingly, we observed that T6SS firing is correlated with rounding of *Pectobacterium* cells, suggesting delivery of a potent cell wall targeting effector. Mutagenesis coupled with functional assays then revealed that a putative T6SS secreted amidase, Tae3^{Pf}, is mainly responsible for MFE01 toxicity towards Pca. Further studies finally demonstrated that Tae3^{Pf} is toxic when produced in the periplasm, and that its toxicity is counteracted by the Tai3^{Pf} inner membrane immunity protein.

INTRODUCTION

Pectobacterium atrosepticum (Pca) ranks in the top 10 soft-rot phytopathogenic bacteria (Mansfield et al., 2012). Pca infects potato plant in cold and temperate countries, causing tuber soft-rot and blackleg disease on the plant stem leading to huge crop production and economic losses (Crépin et al., 2012; Dupuis et al.,

2021; Mansfield et al., 2012; Pérombelon, 2002; Smadja et al., 2004; Toth et al., 2021). After invading plants via wounded sites or natural openings, Pca cells undergo a transition to a pathogenic state, associated with increased growth rate. Following this phase dictated by quorum sensing, Pca secretes a massive amount of plant cell wall degrading enzymes (PCWDEs) to degrade plant tissues (Barnard & Salmond, 2007; Van Gijsegem et al., 2021). Although preventive treatments exist, such as potato seed sterilization or utilization of certified potato seeds, there is no option to cure these deleterious diseases if they occur in the field. One promising answer to combat these phytopathogens is the development of biocontrol strategies using antagonistic microorganisms (Diallo et al., 2011). Among them, bacteria grouped into the term 'Plant Growth-Promoting Rhizobacteria' (PGPR) develop beneficial relationships with plants (Turner et al., 2013). PGPR can directly stimulate plant growth by synthesizing hormones (phytostimulators) or by supplying the plants with nutrients (biofertilizing). Growth stimulation can also be indirectly achieved by suppressing or preventing the deleterious effects of pathogens (Diallo et al., 2011). Among PGPR, fluorescent pseudomonads are well recognized for their beneficial properties to protect plants including biocontrol activities (Haas & Défago, 2005). Most *Pseudomonas* species produce a type VI secretion system (T6SS), a multiprotein transport machine involved in bacterial antagonism (Bernal et al., 2018). By eliminating microbial rivals, the T6SS confers an advantage to adapt to different environmental niches (Gallegos-Monterrosa & Coulthurst, 2021; Gallique, Bouteiller, et al., 2017; Lin et al., 2017).

The T6SS is a widespread apparatus in Gram-negative bacteria (Bingle et al., 2008; Boyer et al., 2009; Cascales, 2008). The T6SS uses a contractile mechanism to inject a needle loaded with effectors directly into target eukaryotic or bacterial cells or to expel effectors into the environment to collect metals (Basler, 2015; Coulthurst, 2019; Hernandez et al., 2020; Ho et al., 2014; Jurenas & Journet, 2021; Yang et al., 2021). The T6SS is comprised of 13 core-component proteins and, in some instances, of additional, accessory subunits. T6SS assembly starts with the formation of the TssJLM membrane complex, which recruits the baseplate that serves as assembly platform to polymerize a tail structure (Cherrak et al., 2019; Cianfanelli et al., 2016; J. Wang et al., 2019). The tubular tail is made of an inner tube wrapped by a sheath structure assembled in an extended conformation. Contraction of the TssBC sheath propels the inner Hcp tube, tipped by a spike and loaded with effectors outside of the cell (Basler, 2015; Brackmann et al., 2017; Cherrak et al., 2019; Cianfanelli et al., 2016; Taylor et al., 2018; J. Wang et al., 2019). A large arsenal of T6SS effectors has been described with a broad repertoire of activities targeting essential macromolecules such as phospholipases, nucleases, proteases, peptidoglycan hydrolases, or ADP-ribosyltransferases (Hernandez et al., 2020; Jurenas & Journet, 2021; Russell et al., 2014).

Among T6SS$^+$ pseudomonads, the *Pseudomonas fluorescens* MFE01 strain was previously shown to secrete Hcp in large amounts, a marker of T6SS functionality (Decoin et al., 2014). Genomic analysis revealed that MFE01 has a single T6SS cluster and several isolated *hcp* and *vgrG* gene islands (Gallique, Decoin, et al., 2017). Previous works showed that MFE01 has antagonistic activity against a wide range of bacterial competitors (Decoin et al., 2014, 2015; Gallique, Decoin, et al., 2017) and participates in motility and collective behaviours (Bouteiller et al., 2020; Gallique, Decoin, et al., 2017). The antibacterial activity of its T6SS confers MFE01 the ability to protect crops, such as potato tubers against some phytopathogens, making MFE01 a promising biocontrol agent (Decoin et al., 2014).

In this study, we carried out tuber assays to provide further insights into the role of MFE01 T6SS for tuber protection and bacterial antagonism against Pca. We then analysed MFE01 T6SS dynamics through time-lapse fluorescence microscopy. Finally, we identified and characterized a major antibacterial effector with putative amidase activity, implicated in Pca antagonism.

EXPERIMENTAL PROCEDURES

Bacterial strains, growth and culture conditions and chemicals

The characteristics of bacterial strains used in this study are presented in Supplemental Table S1. *Escherichia coli* and *P. fluorescens* MFE01 strains were cultivated in Luria Bertani (LB) medium (AES Chemunex) at 37°C and 28°C, respectively. Pca CFBP6276 was grown at 25°C in PGA (Polygatacturonic acid) minimal medium supplemented with 0.4% (w/v) of polygatacturonic acid (Sigma-Aldrich), as described (Barbey et al., 2013). Media were supplemented with antibiotics as appropriate: kanamycin (50 μg/mL for *P. fluorescens* and *E. coli*), gentamycin (20 μg/mL for *P. fluorescens*), tetracycline (10 μg/mL for Pca), rifampicin (50 μg/mL for *P. fluorescens*), chloramphenicol (30 μg/mL for *E. coli*) and ampicillin (100 μg/mL for *E. coli*). For liquid cultures, all bacteria were grown on a rotary shaker at 180 rpm. L-arabinose and isopropyl-β-D-galactopyranoside (IPTG) were purchased from Sigma-Aldrich. *N*-(3-maleimidopropionyl) biocytin (MPB) was purchased from Molecular Probes.

Strain construction

Construction of the MFE01 chromosomal tssB-sfGFP *translational fusion*—A DNA fragment encompassing the 3′ end of the *tssA* gene (460 bp), the complete *tssB*

gene fused to the *sfGFP* sequence and the 5′ end of the *tssC* gene (959 bp) was synthetized by Genewiz, amplified by PCR (oligonucleotides listed in Table S2), and cloned into the *SmaI*-digested pAKE604 suicide vector (El-Sayed et al., 2001). The construct, verified by DNA sequencing, was introduced into *E. coli* S17-1 (Simon et al., 1983) and transferred into *P. fluorescens* MFE01 by biparental mating, as previously described (Decoin et al., 2015). The $_{sf}$*gfp* insertion downstream of the *tssB* gene by a double crossover event was verified by PCR and sequencing.

Construction of the MFE01 Δtae3 *mutant strain*—The markerless *tae3* deletion mutant (Δ*tae3*) was constructed as previously described (Decoin et al., 2015). Briefly, the *tae3* upstream and downstream regions were amplified by PCR (Phusion® High Fidelity DNA polymerase, NEB) using the oligonucleotide pairs muta1amidase/muta2amidase and muta3amidase/muta4amidase (Table S2), respectively. The two fragments were cloned in tandem into the pAKE604 suicide vector before being transferred into MFE01 by biparental mating and selection of the double recombination event. This in-frame *tae3* deletion mutant, containing a truncated version of the *tae3* gene, was checked by PCR analysis and DNA sequencing.

Plasmid construction

Plasmid pJN-Tae3 was constructed by ligation of an *Eco*RI/*Xba*I-digested PCR fragment comprising the *tae3* gene into the pJN105 vector (Newman & Fuqua, 1999) digested by the same enzymes, downstream the arabinose-inducible P*araBAD* promoter. Plasmids pBAD-Tae3^{Pf}-VSVG, pBADtat-Tae3^{Pf}-VSVG and pTrc-ST-Tai3^{Pf}, encoding respectively Tae3^{Pf} fused to a C-terminal VSV-G tag, Tae3^{Pf}-VSVG fused to an N-terminal TorA signal sequence, and Tai3^{Pf} fused to an N-terminal StrepTag, were engineered by restriction-free cloning (van der Ent & Löwe, 2006) as previously described (Aschtgen et al., 2008). Briefly, the fragments encoding Tae3^{Pf} and Tai3^{Pf} were amplified by PCR using oligonucleotides (Table S2) that introduced extensions annealing to the target vector. The double-stranded products of the first PCR were then used as primers for a second PCR using the target vectors (pBAD33, pBAD33tat [D. Jurenas, unpublished vector] and pTrc99A [Pharmacia], respectively) as templates. PCR products were treated with *Dpn*I to eliminate template plasmids and transformed into DH5α-competent cells. For Tae3^{Pf} cloning, plasmids were selected on LB agar plates supplemented with 1% of glucose. Substitutions were introduced by Quikchange site-directed mutagenesis using complementary oligonucleotides bearing the desired mutations. All plasmids have been verified by colony PCR and DNA sequencing.

In vitro antibacterial competition assay

Antibacterial competition assays were carried out as previously published (Murdoch et al., 2011), with slight modification (Decoin et al., 2014). To ensure the selection of attacker and recipient cells for counting, *P. fluorescens* MFE01 strains were transformed with pSMC2.1 (Kan^R; Davey et al., 2003) and Pca CFBP6276 was transformed with pME6000 (Tet^R; Maurhofer et al., 1998). Bacterial cells were grown overnight on LB agar plates and resuspended in LB broth. The optical density at $\lambda = 580$ nm (OD_{580}) was adjusted to 0.5, and cells were mixed in an attacker: recipient ratio of 5:1. About 25-μL drops of the mixture were spotted in triplicate onto 0.22-μm filters deposited onto a prewarmed LB agar plate. After 4 h of incubation at 28°C, bacteria on the filter were resuspended in 1 mL of sterile physiological water and serial dilutions were plated on LB agar supplemented with antibiotic. Colonies were counted after overnight incubation at 28°C.

Biocontrol assays on potato tubers

Solanum tuberosum cv Allians tubers were prepared for inoculation as previously described (Barbey et al., 2013). Inoculation was performed by injection into the intramedulla (to a depth of 1 cm) of 10 μL of a cell suspension containing 10^7 CFU of Pca CFBP6276 and 10^8 CFU of *P. fluorescens* MFE01 WT, Δ*tssC*, Δ*tssC* complemented with a wild-type allele of *tssC* (Δ*tssC-R*; Bouteiller et al., 2020), *tae3* or *tae3* complemented with a wild type allele of *tae3* (*tae3-R*). As controls, tubers were inoculated with each strain alone. Inoculated tubers were incubated in a Minitron incubator (Infors) with 80% humidity at 25°C. Thirty tubers were used per strain or combination. At 1-, 2- and 7-day post-inoculation, 10 tubers for each condition were sectioned across the middle, photographed, analysed by measuring average maceration thickness and cut for bacterial population analysis as previously described (Barbey et al., 2013). Experiments were performed in triplicate. A representative result is shown.

Toxicity assays

For toxicity and rescue assays, *E. coli* DH5α cells were transformed with pBAD33 or derivatives, or co-transformed with pBAD33tat and pTrc99a or derivatives encoding the *tae3* and *tai3* genes, respectively. Transformants were selected on LB agar plates supplemented with 1% of glucose, chloramphenicol, or chloramphenicol and ampicillin. Overnight cultures of transformants were grown in the presence of antibiotics and glucose, serially diluted and 10-μL drops were spotted on LB agar plates supplemented with

antibiotics and 1% of glucose (repression conditions) or 0.2% of arabinose (toxin induction conditions) and 0.5 mM of IPTG (immunity protein induction conditions). Plates were incubated at 37°C for 16 h.

Cell fractionation and membrane differential solubilization

About 10^{10} exponentially growing cells producing $Tai3^{Pf}$ from plasmid pTrc-ST-$Tai3^{Pf}$ were resuspended in 0.5 mL of Tris–HCl 10 mM (pH 8.0), sucrose 30% and incubated for 10 min on ice. After addition of 100 μg/mL of lysozyme and 1 mM of EDTA and further incubation for 45 min on ice, 0.5 mL of Tris–HCl 10 mM (pH 8.0) supplemented with DNase (200 μg/mL) and $MgCl_2$ (4 mM) were added and cells were lysed by five cycles of freeze and thaw. Unbroken cells were removed by centrifugation, and soluble and membrane fractions were separated by ultracentrifugation for 40 min at 100,000*g*. For membrane differential solubilization, the membrane pellet was resuspended in 1 mL of Tris–HCl 10 mM (pH 8.0), EDTA 1 mM supplemented with 1% of sodium *N*-lauroyl sarcosinate (SLS; Sigma-Aldrich) and incubated on a wheel for 1 h at room temperature. SLS is an anionic detergent that selectively disrupts the inner membrane and solubilises inner membrane proteins (Filip et al., 1973). The insoluble (outer membrane) and soluble (inner membrane) fractions were collected by ultracentrifugation at 100,000*g* for 40 min. All samples (Total, Soluble, Total membranes, SLS insoluble and SLS soluble) were resuspended in loading buffer and analysed by SDS-PAGE and immunoblotting using anti-StrepTag (Classic, Bio-Rad). Anti-IscS, anti-TolA and anti-OmpA antibodies (laboratory collection) were used as cytoplasmic, inner membrane and outer membrane markers, respectively.

Substituted cysteine accessibility method

Topology assays using cysteine accessibility experiments were carried out as described (Aschtgen et al., 2010; Bogdanov, 2017) with modifications. Positions of the cysteine substitutions were based on (i) DeepTMHMM prediction of potential transmembrane segments (https://www.biorxiv.org/content/10.1101/2022.04.08.487609v1) and (ii) serine residues (to limit impact of substitutions on $Tai3^{Pf}$ function). 2×10^{10} cells producing the cysteine variant were harvested, resuspended in buffer A (Hepes 100 mM pH 7.5, sucrose 250 mM, $MgCl_2$ 25 mM and KCl 0.1 mM) to a final OD_{600} of 12. 3-(*N*-maleimidyl-propionyl) biocytin (MPB; Molecular Probes) was added to a final concentration of 100 μM (from a 20 mM stock freshly dissolved in DMSO) and the cells were incubated for 30 min at 25°C. β-Mercaptoethanol (20 mM final concentration) was added to quench the biotinylation reaction, and the cells were washed and resuspended in buffer A supplemented with 5 mM *N*-ethyl maleimide (Sigma-Aldrich) to block all free sulfhydryl residues. After incubation for 20 min at 25°C, cells were disrupted by sonication. Membranes recovered by ultracentrifugation for 40 min at 100,000*g* were resuspended in 1 mL of buffer B (Tris–HCl 10 mM pH 8.0, NaCl 100 mM and Triton X-100 1% (v/v)) supplemented with protease inhibitor cocktail (Complete, Roche). After incubation on a wheel for 1 h, insoluble material was discarded by centrifugation 15 min at 20,000*g*, and solubilized proteins were subjected to precipitation with 100 μL of Strep-Tactin Superflow resin (IBA Technology) equilibrated in buffer B. After 1 h of incubation on a wheel, and five washes with 1 mL of buffer B, Strep-tagged $Tai3^{Pf}$ was eluted with 100 μL of buffer B supplemented with 2.5 mM of desthiobiotin, boiled in Laemmli buffer before SDS-PAGE analysis and immuno-detection with anti-StrepTag antibodies (to detect the proteins) or streptavidin (to detect the biotinylated proteins) coupled to alkaline phosphatase. Control experiments were performed on purified membranes instead of whole cells.

Fluorescence microscopy and data analysis

Bacterial cells grown overnight in LB media were harvested and resuspended in LB to an OD_{600} of 10. Cell resuspension or mixtures were then spotted on a thin 2% agarose pad containing LB, covered with a coverslip and incubated for 2–5 min at 28°C before microscopy acquisition. Fluorescence microscopy analysis was performed with a Nikon Eclipse Ti2 microscope equipped with an OrcaFusion digital camera (Hamamatsu) and a perfect focus system to automatically maintain focus to keep the point of interest within the specimen in sharp focus at all times despite mechanical or thermal perturbations. The microscope temperature was maintained at 30°C in a thermoregulated incubator. All fluorescence images were acquired with a minimal exposure time to minimize bleaching and phototoxicity effects. Exposure times were typically 200 ms for phase contrast and 20 ms for fluorescent fusions. The images shown in the figures are representative regions cropped from large fields and are from at least triplicate experiments. Images were analysed using ImageJ (C. A. Schneider et al., 2012). For analysis of Pca cell lysis, Pca and *P. fluorescens* MFE01 cells were mixed in a 1:1 ratio, disposed on an agar pad and followed using time-lapse fluorescence microscopy over a 4-h period. Pca cells that remained intact and the cells that lysed (including those lysing after

rounding) were then numbered from five different fields (40–100 Pca cells per field), and the experiments were performed four times.

Statistical analyses

The Mann and Whitney test was used to assess differences in maceration symptoms between groups (p-value < 0.05). The one-way ANOVA test was used to

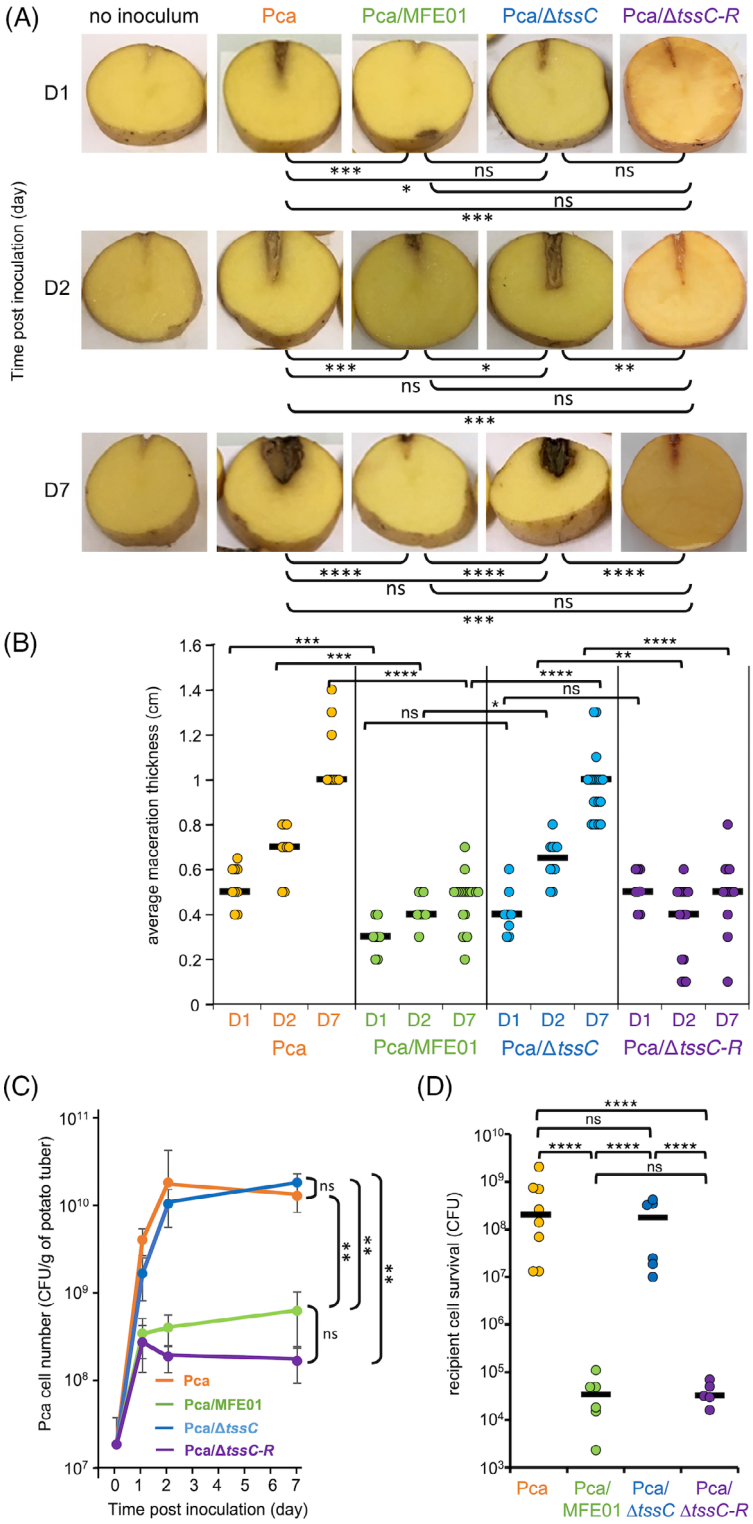

FIGURE 1 Legend on next page.

assess differences in prey recovery cells between groups (p-value < 0.05).

RESULTS

A functional T6SS is required for MFE01 to protect potato tubers against Pca

Previous data have shown that the *P. fluorescens* MFE01 *hcp2* gene, which encodes the major Hcp protein secreted in the medium, is important to confer protection of potato tubers against the phytopathogen Pca (Decoin et al., 2014). Due to the wealth of *hcp* genes in the *P. fluorescens* MFE01 genome (Figure S1) and their potential redundancy, we tested the role of the T6SS in potato tuber protection by carrying out *in planta* assays using a mutant of a gene essential for T6SS function, *tssC*. For this, bacterial suspensions containing 2×10^7 Pca CFU per gram of potato tuber were inoculated into a wounded site, and the development of soft-rot symptoms was evaluated over a 7-day period (Figure 1A,B). When inoculated alone, Pca caused maceration of potato tubers, with damages appearing as soon as 2 days after inoculation. Maceration intensity increased with incubation time. When Pca was mixed with wild-type (WT) *P. fluorescens* MFE01, only maceration damages comparable to the wound in the absence of inoculum were observed, demonstrating that MFE01 protects the tuber against Pca. This protection is dependent on a functional T6SS, as co-inoculation of Pca with MFE01 Δ*tssC* cells did not prevent potato tuber maceration, with damages similar to inoculation with Pca alone. To measure the impact of MFE01 on Pca population, we counted surviving Pca CFU on selective plates (Figure 1C). When inoculated alone or mixed with MFE01 Δ*tssC* mutant cells, the Pca population reached $\sim 10^{10}$ CFU/g of potato tuber after 2 days and then stabilized. In contrast, when mixed with WT MFE01, the Pca population reached 10^9 CFU/g of potato tuber. These results suggest that the MFE01 T6SS partly inhibits the growth of Pca *in planta*. This conclusion is supported by in vitro experiments demonstrating that Pca survival is severely affected by MFE01 in a T6SS-dependent manner (Figure 1D). Taken together, these data show that MFE01 deploys its T6SS to eliminate Pca cells, or to affect their growth, hence limiting Pca density in the potato tuber and the development of the disease.

MFE01 T6SS activity causes Pca and *E. coli* cell rounding and lysis

To visualize T6SS sheath activity, we constructed a translational fusion between a component of the T6SS sheath, TssB and the superfolder green fluorescent protein (sfGFP). This fusion was engineered on the MFE01 chromosome, at the native locus. We then monitored T6SS sheath dynamics by time-lapse fluorescence microscopy (Figure 2A, Video S1). MFE01 cells assemble 5 sheaths in average and up to 12 sheaths per cell (Figure 2B) with dynamics similar to other species such as *Vibrio cholerae*, *Serratia marcescens* or enteroaggregative *E. coli* (EAEC) (Basler et al., 2012; Brunet et al., 2013; Gerc et al., 2015; Santin et al., 2018, 2019; J. P. Schneider et al., 2019): assembly in ∼60 s (Figure 2C) and a residence time of ∼3 min (Figure 2D). To determine whether MFE01 T6SS presents a defensive (i.e., respond to an attack) or aggressive (i.e., fire against any cell in contact) behaviour, we then compared T6SS activity in single cells and cells established in microcolonies. The recordings and statistical analyses showed that there are no significant differences in the number of sheath assemblies (Figure 2E), contraction events (Figure 2F) or residence time (Figure 2G) when cells are isolated or in contact with other cells. These observations suggest that *P. fluorescens* MFE01 can be considered as an aggressive strain, with its T6SS categorized as an offensive weapon.

FIGURE 1 MFE01 prevents potato tuber maceration by deploying its T6SS against Pca. Biocontrol activity of *Pseudomonas fluorescens* MFE01 wild-type (WT) (MFE01), *P. fluorescens* Δ*tssC* (Δ*tssC*) and Δ*tssC* producing TssC (Δ*tssC-R*) were monitored against Pca (Pca) for a 7-day period. Visual damages, Pca population and maceration thickness were assessed on Day 1 (D1), Day 2 (D2) and Day 7 (D7). (A) Potato tuber protection assay on a 7-day period was realized with different inoculation conditions: control (no inoculum, 0.9% NaCl solution), Pca alone (lane 1), Pca versus MFE01 (lane 2), Pca versus MFE01 Δ*tssC* (lane 3) and Pca versus MFE01 Δ*tssC* producing TssC (Δ*tssC-R*, lane 4). (B) Maceration thickness analysis of potato tubers 1, 2 and 7 days after inoculation of Pca alone (orange), Pca versus MFE01 (green), Pca versus MFE01 Δ*tssC* (blue) and Pca versus MFE01 Δ*tssC* producing TssC (Δ*tssC-R*, purple). Horizontal bars represent the median of the data points. Significant differences are indicated with asterisks (Mann and Whitney test, *, p-value < 0.05; **, p-value < 0.01; ***, p-value < 0.001; ****, p-value < 0.0001; ns, not significant; $n = 5$–16). (C) Numeration of Pca density (CFU/g fresh weight of potato tubers) after inoculation of Pca alone (orange), Pca versus MFE01 (green), Pca versus MFE01 Δ*tssC* (blue) and Pca versus MFE01 Δ*tssC* producing TssC (Δ*tssC-R*, purple) in potato tubers, monitored on Days 1, 2 and 7. Curves represent the mean value of triplicates with standard deviations. Significant differences are indicated with asterisks (Mann and Whitney test, *, p-value < 0.05; **, p-value < 0.01; ***, p-value < 0.001; ****, p-value < 0.0001; ns, not significant; $n = 3$). (D) MFE01 antibacterial activity against Pca in vitro. Number of surviving Pca cells after culture alone (orange), or co-culture with MFE01 (green), MFE01 Δ*tssC* (blue) or MFE01 Δ*tssC* producing TssC (Δ*tssC-R*, purple) for 4 h at 25°C. Horizontal bars represent the median of the data points. Significant differences are indicated with asterisks (one-way ANOVA test, *, p-value < 0.05; **, p-value < 0.01; ***, p-value < 0.001; ****, p-value < 0.0001; ns, not significant; $n = 5$–8).

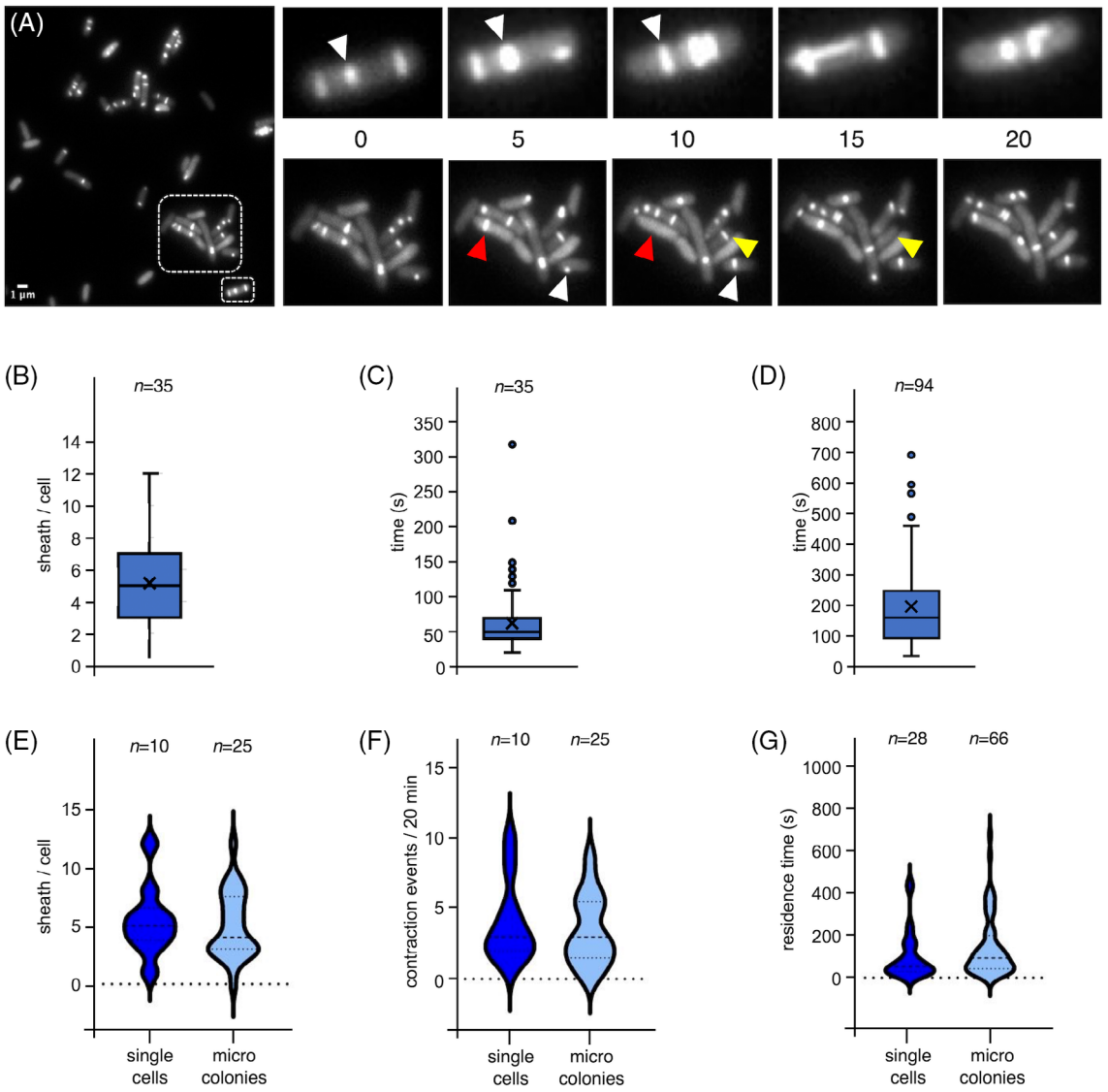

FIGURE 2 MFE01 assembles highly dynamic T6SS with aggressive behaviour. (A) Representative fluorescence microscopy field of MFE01 TssB-sfGFP (scale bar, 1 µm) (left panel) and time-lapse fluorescence recordings of a single cell (upper panels) and microcolony (lower panels) (time in min). White arrowheads indicate T6SS sheath assembly events. Red and yellow arrowheads indicate contraction events. The corresponding video is provided in the Supporting Information (Video S1). (B–D) T6SS sheath dynamics. Box plot representation of the number of T6SS sheath per cell (B), of the assembly time (time necessary to assemble an extended sheath, C) and of the residence time (time for which the sheath remains extended before contraction, D). The internal horizontal line and cross represent the median and mean values, respectively; the boundaries of the internal box plot correspond to the 25th and 75th percentiles; the whiskers correspond to the 10th and 90th percentiles. Outliers are shown as closed circles. The number of analysed events (*n*) is indicated on the top of each graph. (E–G) Comparison of T6SS sheath dynamics in single cells and microcolonies. Violin plot representations representing the number of sheath per cell (E), the number of contraction events per cell over a 20-min period (F), and the residence time (G) of MFE01 TssB-sfGFP single cells (dark blue) or microcolonies (light blue). The distribution is represented by the outer shape. The broken line represents the median value. The dotted lines of the internal violin plot correspond to the 25th and 75th percentiles, respectively. The number of analysed events (*n*) is indicated on the top of each graph.

To gain information on the impact of MFE01 T6SS activity on target cells, MFE01 TssB-sfGFP cells were mixed with Pca cells in a 1:1 ratio, and analysed by time-lapse fluorescence microscopy. Figure 3A shows that Pca cells in contact with WT MFE01 change morphology, from a rod to a spherical shape (see white and orange arrows), before losing cytoplasmic density (Figure 3A, Video S2). Quantitative analyses further showed that about 35% of Pca cells lysed when in contact with MFE01 over a 4-h period, with ~80% of these Pca cells experiencing cell rounding before lysis (Figure 3B). While cell rounding was the most frequent consequence, we also observed blebbing, plasmolysis and burst events (Figure S2). The morphological modification and lysis of Pca cells were not observed when co-cultured with MFE01 Δ*tssC* cells (Figure 3A,B, Video S3). Interestingly, target cell rounding appears after sheath contraction suggesting that Pca damages

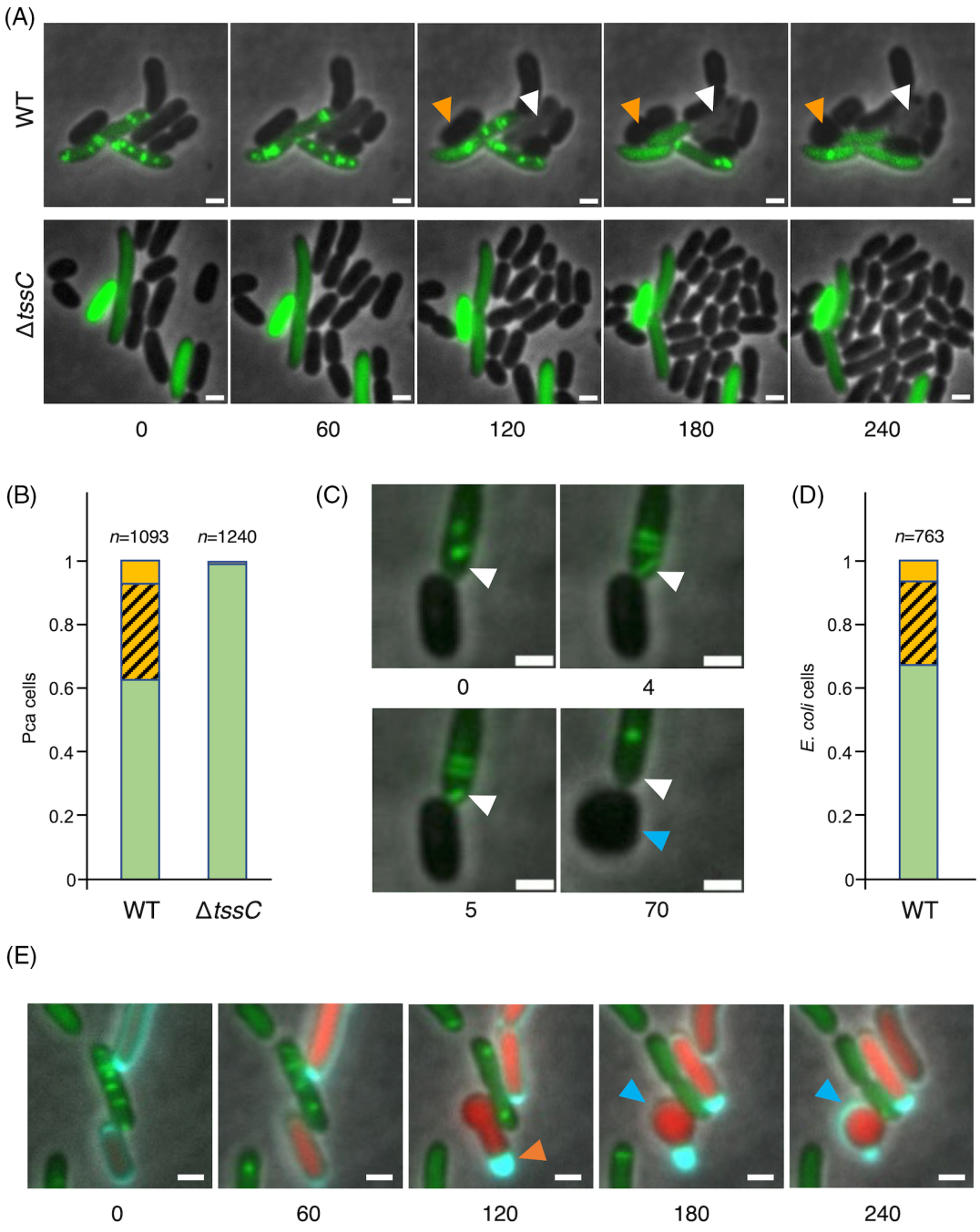

FIGURE 3 Microscopic analysis of MFE01 T6SS antibacterial activity. (A) Time-lapse fluorescence microscopy recordings of *Pseudomonas fluorescens* MFE01 wild-type (WT) or Δ*tssC* producing TssB-sfGFP against Pca (time in min). White and orange arrowheads indicate events of Pca cell damage (scale bar, 1 μm). Corresponding videos are provided in the Supporting Information (Videos S2 and S3). (B) Histograms reporting antibacterial activity of MFE01 WT and MFE01 Δ*tssC* against Pca after a 4-h incubation (green, living cells; orange, lysed cells; hatched orange, lysis following rounding). Only bacteria in contact with MFE01 or Δ*tssC* were counted. The number of analysed cells (*n*) is indicated on the top of each graph. (C) Time-lapse fluorescence microscopy recordings of *P. fluorescens* MFE01 TssB-sfGFP in contact with Pca (time in min) (scale bar, 1 μm). White arrowheads point an event of T6SS sheath assembly and contraction. The blue arrowhead highlights Pca cell rounding. The corresponding video is provided in the Supporting Information (Video S4). (D) Histograms reporting antibacterial activity of WT MFE01 against *Escherichia coli* after a 4-h incubation (green, living cells; orange, lysed cells; hatched orange, lysis following rounding). Only *E. coli* in contact with MFE01 were counted. The number of analysed cells (*n*) is indicated on the top of each graph. (E) Time-lapse fluorescence microscopy recordings of *P. fluorescens* MFE01 TssB-sfGFP (green) against *E. coli* producing mTurquoise in the periplasm and mCherry in the cytoplasm (time in min) (scale bar, 1 μm). The orange and blue arrows point to periplasm collapse at the cell pole and cell rounding, respectively. Corresponding videos are provided in the Supporting Information (Videos S5 and S6).

might be correlated with a T6SS firing event (Figure 3C, Video S4). Similar observations were made when MFE01 was co-cultured with *E. coli* K12 (Figure 3D). As we observed that Pca and *E. coli* rounding is the major phenotype associated with *P. fluorescens* MFE01 T6SS antibacterial activity and that cell rounding is usually associated with cell wall damages, these data suggest that the MFE01 T6SS delivers one or several effectors targeting the peptidoglycan.

To better visualize the cellular consequences of MFE01 on target cells, we performed fluorescence microscopy experiments using a strain of *E. coli* harbouring plasmid pTHV037dsbA-SP-msfTq2O_sol-Cytomcherry as recipient. This strain produces mCherry in the cytoplasm and sfTurquoise in the periplasmic space, allowing to differentiate the two compartments (Deghelt et al., 2023). Time-lapse fluorescence microscopy recordings showed that upon MFE01 T6SS firing, the periplasm of the attacked cell collapsed at one pole of the cell, eventually reached the other pole, before cell rounding (Figure 3E, Videos S5 and S6). Taken together, these images suggest that the peptidoglycan of the recipient cell is severely damaged after an MFE01 T6SS attack.

MFE01 delivers a putative amidase of the Tae3 family that is active against Pca and *E. coli*

Based on the previous observations, we searched for a potential effector targeting the peptidoglycan. T6SS effectors have been found to be additional domains associated with the Hcp, VgrG or PAAR proteins, or being independent proteins encoded at vicinity of *hcp*, *vgrG* or *paar* genes (Hernandez et al., 2020; Jurenas & Journet, 2021). We therefore conducted a bioinformatic survey to identify *hcp*, *vgrG* and *paar* genes and analysed their sequences and their genomic neighbourhoods (Figure S1). In addition to the main T6SS gene cluster containing a copy of the *vgrG* gene, we found one *hcp*, five *vgrG* and three *hcp-vgrG* islands (Figure S1). These islands encode putative effectors with various functions, including DNases, phospholipases, peptidases, PoNE-like phosphodiesterases and Rhs proteins (Figure S1). Interestingly, one of the *hcp-vgrG* islands encodes a putative amidase effector of the Tae3 family (called hereafter Tae3^{Pf}) (Figure 4A). This gene is located downstream *hcp3* and is followed by a gene of unknown function and a potential additional effector-immunity pair (Figure 4A).

To test whether Tae3^{Pf} is involved in MFE01 antibacterial activity, we engineered an in-frame deletion of the *tae3* gene on the MFE01 chromosome and tested the ability of MFE01 Δ*tae3* cells to cause Pca and *E. coli* cell rounding and lysis. Time-lapse fluorescence microscopy recordings showed that MFE01 Δ*tae3* cells assemble dynamic sheath structures at levels comparable to the wild-type strain (Figure S3A,B), indicating that the T6SS remains active in the absence of Tae3^{Pf} and that Tae3^{Pf} is not required for functional assembly of the T6SS. Figure 4B shows that the *tae3* mutation decreases MFE01 antibacterial activity against Pca in vitro but maintains a significant level of activity, suggesting that other potential effectors contribute to Pca killing. It is worth noting that the (over)production of Tae3 in the Δ*tae3* mutant strain significantly increases T6SS activity compared to the wild-type strain (Figure 4B). One may hypothesize that more Tae3 are loaded and delivered into Pca cells, increasing the potential of MFE01. These data were confirmed by time-lapse microscopy recordings of Pca or *E. coli* incubated with MFE01 Δ*tae3* cells. While some Pca and *E. coli* cell lysis events could be still observed in the absen (Figure 4C,D, Videos S7 and S8), quantitative analyses revealed a significant reduction in antibacterial activity with 8%–15% of Pca and *E. coli* lysed cells over a 4-h period (Figure 4E; to compare with ∼35% of lysis with WT MFE01; see Figure 3B). This decrease of T6SS activity was also accompanied by a reduction in the number of rounding events in both Pca and *E. coli* (Figure 4E). Potato tuber assays further showed that Pca co-inoculation with *tae3* mutant cells do not confer tuber protection against Pca, although the maceration intensity was significantly decreased compared to Pca alone (Figure 4F,G). As shown in the in vitro antibacterial assay, (over)production of Tae3 significantly increases potato tuber protection compared to the WT strain (Figure 4F,G). Taken together, these results confirm that the Tae3 putative amidase is an important T6SS effector in MFE01 and that the remaining antibacterial activity could be attributed to other potential effectors secreted through the T6SS.

Tae3^{Pf} is toxic in the periplasm of *E. coli* and its toxicity is counteracted by the Tai3^{Pf} inner membrane immunity protein

To test whether the putative Tae3^{Pf} amidase has toxic activity, the *P. fluorescens* MFE01 *tae3* gene was cloned into the pBAD33 vector, fused, or not, to the TorA Tat signal sequence for its export into the periplasm. Figure 5A shows that the Tae3^{Pf} production in the cytoplasm has no impact on *E. coli* growth, while the production of Tae3^{Pf} in the periplasm of *E. coli* is toxic in the presence of arabinose. Substitution of the cysteine and histidine residues of the putative catalytic site of Tae3^{Pf} inactivated the toxin (Figure 5A), although these variants were produced at levels comparable to WT Tae3^{Pf} (Figure 5B). Genes encoding T6SS toxins are usually genetically linked to genes that confer immunity against the activity of the toxin (Durand

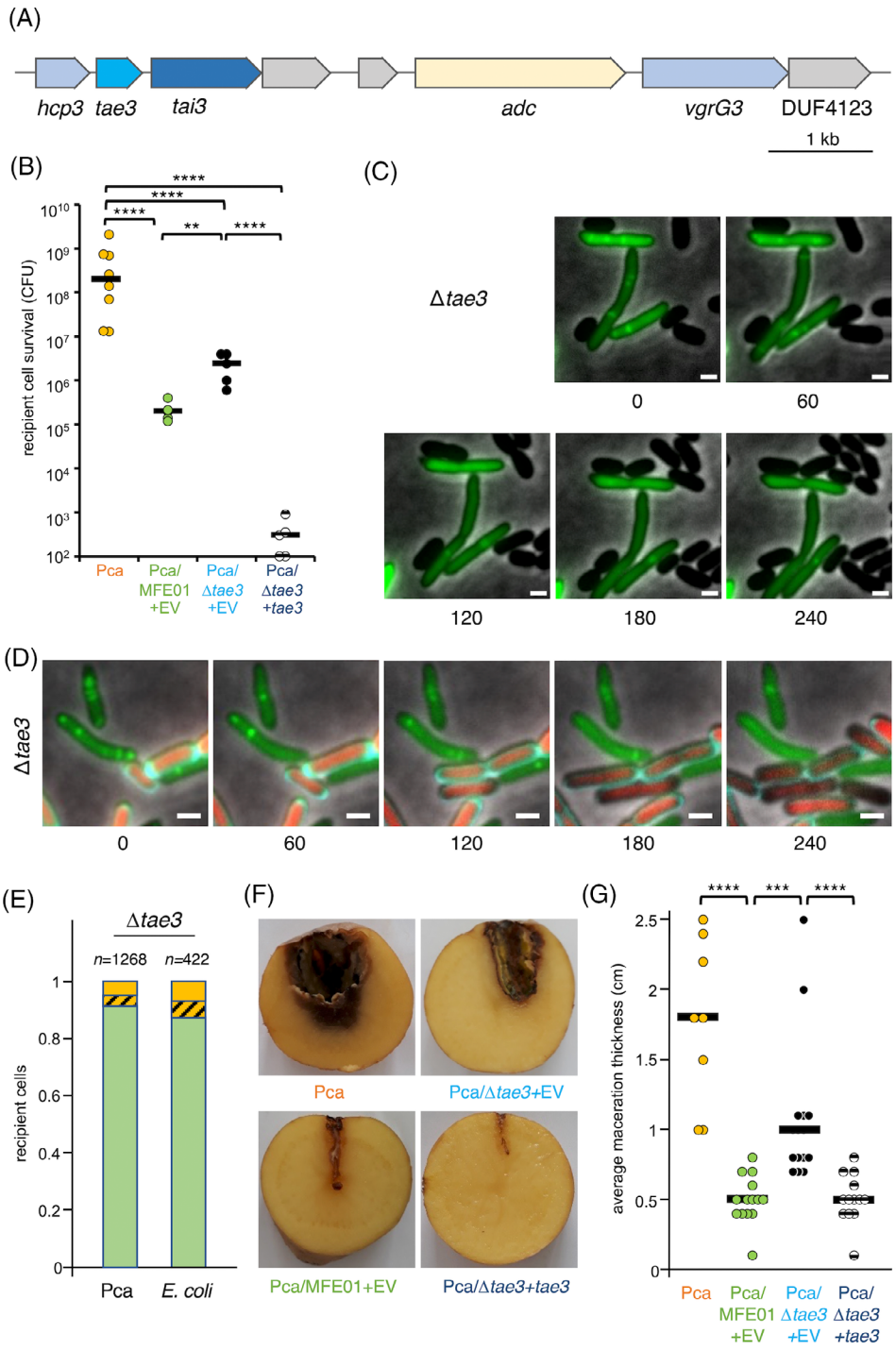

FIGURE 4 The Tae3 amidase is an important MFE01 T6SS effector. (A) Schematic representation of the *hcp3-vgrG3* genomic island. The genes with identified function are indicated in colour. The gene encoding a putative arginine decarboxylase (*adc*) is coloured in yellow. Uncharacterized genes are indicated in grey. (B) MFE01 antibacterial activity against Pca in vitro. Number of surviving Pca cells after culture alone (orange), or co-culture with MFE01 (with the pJN105 empty vector [EV], green), MFE01 Δ*tae3* (with EV, blue) or MFE01 Δ*tae3* producing Tae3 (dashed blue) for 4 h at 25°C. Horizontal bars represent the median of the data points. Significant differences are indicated with asterisks (one-way ANOVA test; *, *p*-value < 0.05; **, *p*-value < 0.01; ***, *p*-value < 0.001; ****, *p*-value < 0.0001; ns, not significant; $n = 5–8$). (C, D) Time-lapse fluorescence microscopy recordings of *Pseudomonas fluorescens* MFE01 Δ*tae3* producing TssB-sfGFP against Pca (C) or *Escherichia coli* producing mTurquoise in the periplasm and mCherry in the cytoplasm (D) (time in min) (scale bar, 1 μm). Corresponding videos are provided in the Supporting Information (Videos S7 and S8). (E) Histograms reporting antibacterial activity of MFE01 Δ*tae3* against Pca or *E. coli* after a 4-h incubation (green, living cells; orange, lysed cells; hatched orange, lysis following rounding). Only bacteria in contact with MFE01 Δ*tae3* were counted. The number of analysed cells (*n*) is indicated on the top of each graph. (F, G) Biocontrol activity of *P. fluorescens* MFE01 WT (with EV, MFE01 + EV), *P. fluorescens* Δ*tae3* (with EV, Δ*tae3* + EV) and Δ*tae3* producing Tae3 from pJN105 (Δ*tae3* + tae3) were monitored against *Pectobacterium atrosepticum* (Pca) for a 7-day period. Visual damages, Pca population and maceration thickness, were assessed on Day 7. (F) Potato tuber protection assay with Pca alone, Pca and MFE01 + EV, Pca and MFE01 Δ*tae3* + EV and Pca and MFE01 Δ*tae3* + tae3. (G) Maceration thickness analysis of potato tubers after inoculation of Pca alone (orange), Pca and MFE01 + EV (green), Pca and MFE01 Δ*tae3* + EV (blue) and Pca and MFE01 Δ*tae3* + tae3 (dashed blue). Horizontal bars represent the median of the data points. Significant differences are indicated with asterisks (Mann and Whitney test, *, *p*-value < 0.05; **, *p*-value < 0.01; ***, *p*-value < 0.001; ****, *p*-value < 0.0001; ns, not significant; $n = 8–14$).

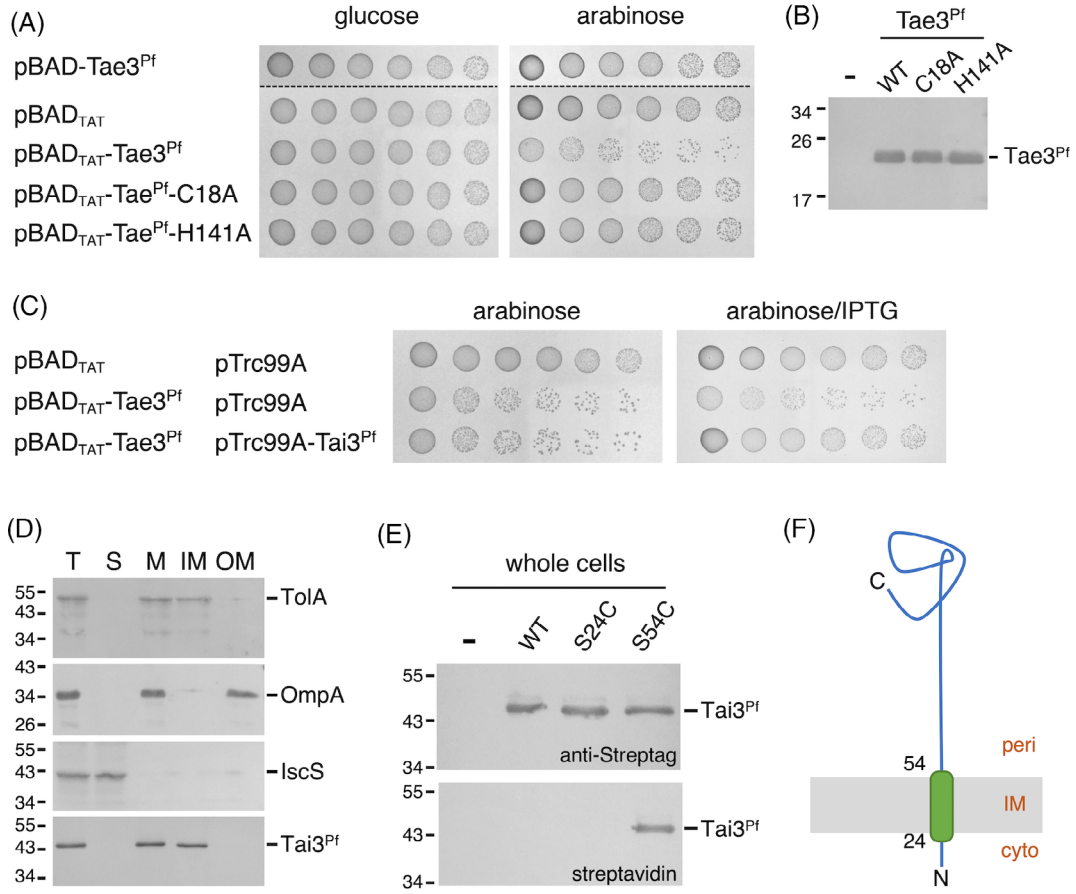

FIGURE 5 Tae3^{Pf} toxicity in *Escherichia coli* is counteracted by the Tai3^{Pf} inner membrane immunity protein. (A) Toxicity assay in the heterologous host *E. coli*. Cultures of *E. coli* cells bearing the pBAD33 plasmid-producing Tae3^{Pf} (cytoplasm), the empty pBAD33tat plasmid or the pBAD33tat plasmid-producing wild-type (WT) or catalytic mutants (C18A or H141A) of Tae3^{Pf} (exported to the periplasm) were serially diluted and 10^{-1} to 10^{-6} dilutions (from left to right) were spotted on LB-agar plates supplemented with 1% of glucose or 0.2% of L-arabinose to repress or induce expression from pBAD33tat vectors, respectively. (B) Western-blot analyses of WT and catalytic mutants of Tae3^{Pf}. Cell extracts of *E. coli cells* producing WT or catalytic mutants (C18A or H141A) of Tae3^{Pf} were analysed by SDS-PAGE, transferred onto nitrocellulose and immunodetected with anti-VSV-G monoclonal antibodies. Molecular weight markers are indicated on the left. (C) Toxicity and rescue assays in the heterologous host *E. coli*. Cultures of *E. coli* cells bearing the empty or *tae3*-encoded pBAD33tat plasmid and the empty or *tai3*-encoded pTrc99A plasmid were serially diluted and 10^{-1} to 10^{-6} dilutions (from left to right) were spotted on LB-agar plates supplemented with 0.2% of L-arabinose to induce expression of *tae3*, or supplemented with 0.2% of L-arabinose and 0.5 mM of IPTG to induce expression of *tae3* and *tai3*, respectively. (D) Cell fractionation and differential solubilization. *E. coli* cells producing Strep-tagged Tai3^{Pf} (T) were subjected to cell fractionation to separate the soluble (S) from the membrane (M) fraction. The membrane fraction was then solubilized with SLS to separate inner (IM) and outer (OM) membranes. The different fractions were analysed by SDS-PAGE, transferred onto nitrocellulose and immunodetected, from top to bottom, with anti-TolA, anti-OmpA, anti-IscS and anti-Strep-Tag (Tai3^{Pf}) antibodies. Molecular weight markers are indicated on the left. (E) Substituted cysteine accessibility method. *E. coli* cells producing Strep-tagged wild-type (WT) or S24C or S54C Tai3^{Pf} were treated with MPB to label accessible thiol groups. After Tai3^{Pf} precipitation, the samples were analysed by SDS-PAGE, transferred onto nitrocellulose and immunodetected with anti-StrepTag monoclonal antibodies (upper panel) and streptavidin coupled to alkaline phosphatase (lower panel). Molecular weight markers are indicated on the left. (F) Topological model of Tai3^{Pf}. The inner membrane (IM), which separates the cytoplasm (cyto) from the periplasm (peri), is indicated as well as the boundaries of the Tai3^{Pf} transmembrane segment (green).

et al., 2014; Jurenas & Journet, 2021; Russell et al., 2014). Indeed, co-expression of the gene located downstream of *tae3*, called hereafter *tai3^{Pf}*, protects *E. coli* from the action of Tae3^{Pf} (Figure 5C). Subcellular localization of the Tai3^{Pf} immunity protein showed that it cofractionates with membrane proteins (Figure 5D). Further differential membrane solubilization with sodium lauroyl-sarcosinate, a detergent that specifically solubilize inner membrane proteins (Filip et al., 1973), demonstrated that Tai3^{Pf} associates with the inner membrane (Figure 5D). Bioinformatic analyses suggest that Tai3^{Pf} comprises a single transmembrane segment between residues 29 and 51. To test this topological model, we performed the substituted cysteine accessibility method, which consists to probe cysteine thiol groups with *N*-(3-maleimidopropionyl) biocytin (MPB), a compound that readily crosses the outer membrane but unable to reach the cytoplasm (Bogdanov, 2017). We substituted serine residues located at positions 24 and 54 with cysteines. These

Tai3^{Pf} variants were functional as they conferred protection against Tae3^{Pf} (Figure S4A), were produced at similar levels (Figure S4B), and are accessible (Figure S4C). Figure 5E shows that the S24C variant is not labelled while the S54C variant is labelled with MPB, confirming the presence of a transmembrane segment between these two positions, in an in-to-out topology (Figure 5F).

DISCUSSION

There are increasing evidence that T6SSs are useful tools for bacteria to adapt and to colonize specific niches (Alcoforado Diniz et al., 2015; Allsopp et al., 2020; Chassaing & Cascales, 2018; Gallegos-Monterrosa & Coulthurst, 2021). Several studies have shown that the T6SS allows bacteria to outcompete other microbial rivals to survive and persist in their environment (Allsopp et al., 2020; Chen et al., 2019; Fu et al., 2013; Kapitein & Mogk, 2013; Ma et al., 2014; Miller, 2013; Sana et al., 2016; Yang et al., 2021). T6SS gene clusters are commonly found in commensal and pathogenic plant-associated bacteria (Bernal et al., 2018), including members of *Agrobacterium*, *Pectobacterium*, *Ralstonia*, *Acidovorax*, *Pseudomonas*, *Xanthomonas* or *Azospirillum* genera (Bayer-Santos et al., 2018; Bernal et al., 2017; Cassan et al., 2021; Ceseti et al., 2019; Durán et al., 2021; Liu et al., 2008; Ma et al., 2014; Tian et al., 2015; Zhang et al., 2012). In phytopathogens, the T6SS antagonizes other plant-associated bacteria to colonize the niche and to have access to plant entry sites. In commensals or symbionts, the T6SS helps to protect the plant against phytopathogens and may stimulate plant defences and fitness (Bernal et al., 2018).

In this study, we showed that *P. fluorescens* MFE01 protects potato tubers against Pca and that this protection is promoted by its T6SS. This result confirms a previously published work defining one of the MFE01 *hcp* genes, *hcp2*, as an important determinant for potato protection (Decoin et al., 2014). A protective role of the T6SS was also shown in other PGPR belonging to the *Pseudomonas* genus. For example, *P. protegens* uses T6SS to exert antagonist activity against insect pathogens (Vacheron et al., 2019), *P. fluorescens* F113 and Pf29Arp T6SSs increase persistence in the rhizosphere and present antagonistic activity against fungi, respectively; while *P. putida* exerts a T6SS-dependant biocontrol activity against *Xanthomonas campestris* which is responsible for *Nicotinia benthamiana* leaf necrosis (Bernal et al., 2017; Durán et al., 2021; Marchi et al., 2013).

It is interesting to note that our quantification analyses showed that Pca density in the potato tuber in the presence of MFE01 is only a log below the pathogen population when alone or in the presence of MFE01 Δ*tssC*. However, even such a limited difference has a significant impact on potato tuber maceration. As previously described with another biocontrol strain, *Rhodococcus erythropolis*, Pca has to reach a certain density, i.e. the quorum, to initiate a strong and synchronized PCWDE production leading to tissues maceration (Chane et al., 2019). For Pca, this density was estimated above 5.10^9 CFU/g of potato tuber (Chane et al., 2019). One may hypothesize that MFE01 deploys its T6SS to prevent Pca from reaching this density, and hence to prevent massive PCWDE production.

These *in planta* results were corroborated with data showing that MFE01 T6SS limits Pca and *E. coli* growth in co-cultures. However, it should be noted that the MFE01 T6SS-dependent impact on Pca differs in the potato tubers (elimination of half the population) compared to the in vitro activity (3–4 logs of antibacterial activity); this could be attributable to the presence of caches and crevices in the tuber parenchyma, which limits cell-to-cell contacts between the two strains.

Further time-lapse fluorescence microscopy recordings showed that MFE01 cells assemble five T6SS structures per cell on average and that, once assembled, these sheath structures remain extended for several minutes. As previously shown for *V. cholerae*, *S. marcescens* or EAEC (Basler et al., 2012; Brunet et al., 2013; Gerc et al., 2015; Ostrowski et al., 2018; Santin et al., 2018), MFE01 T6SS activity presents an aggressive behaviour. In co-culture, MFE01 T6SS activity leads to Pca or *E. coli* lysis, mainly through rounding of the target cell. Other cell damage consequences were also observed, such as blebbling, plasmolysis or burst. Similar lysis phenotypes were shown to be associated with *V. cholerae* T6SS activity (Basler et al., 2012). Analyses of the time-lapse images showed that target cell rounding correlated with T6SS contraction events, suggesting that T6SS translocates effector(s) targeting the cell wall. Indeed, peptidoglycan, which is one of the major structural components of the cell envelope that confers bacterial shape, is a common target for antibacterial strategies (Russell et al., 2014). T6SS effectors that target the peptidoglycan belong to enzymes of the amidase (Tae; hydrolysing peptide cross bridges) and glycoside hydrolase (Tge, hydrolysing the glycan backbone) families (Durand et al., 2014; Hernandez et al., 2020; Jurenas & Journet, 2021; Russell et al., 2014). In each family, Tae and Tge effectors segregate into subfamilies that diverge by the specific bridge they target. Based on the usual genomic environment of T6SS effector genes, we screened the MFE01 genome and identified a putative amidase of the Tae3 family, encoded downstream of an *hcp* gene in an *hcp-vgrG* island, and located upstream of a gene of unknown function. Peptidoglycan-targeting enzymes have been shown to be common T6SS effectors in pseudomonads, including the opportunistic pathogen

P. aeruginosa (Chou et al., 2012; Radkov et al., 2022; Russell et al., 2011, 2012; T. Wang et al., 2020; Whitney et al., 2013). While MFE01 T6SS antibacterial activity and T6SS-mediated potato protection are not abolished in a strain lacking Tae3, our results showed that Tae3^{Pf} contributes significantly to Pca and *E. coli* rounding and lysis. Tae3^{Pf} is indeed toxic when produced in the periplasm of *E. coli* and its toxicity is counteracted when the gene located downstream *tae3* is co-expressed. This gene, which likely encodes a specific immunity to Tae3^{Pf}, was named *tai3*. Tai3^{Pf} is an inner membrane protein with a single transmembrane pass with in-to-out topology, and the majority of the protein locates in the periplasm. One may hypothesize that this periplasmic domain is responsible for neutralizing Tae3^{Pf} activity, likely by protein–protein interaction.

Due to the large number of highly dynamic T6SSs assembled per cell and their aggressive behaviour, MFE01 is likely to colonize very efficiently plants and soils by eliminating microbial rivals. Indeed, our results provide evidence for the important role of the T6SS in the biocontrol properties of *P. fluorescens* MFE01, which can be considered/envisioned as an alternative strategy to defeat phytopathogens and to protect plants. Interestingly, *P. fluorescens* MFE01 carries a single T6SS gene cluster and nine *hcp*, *vgrG* or *hcp-vgrG* islands, which encode >15 potential effector-immunity pairs. Characterization of the MFE01 effector repertoire will likely reveal the variety of activities and potential targets, and probably the broad potential of MFE01 for biocontrol.

AUTHOR CONTRIBUTIONS

Yvann Bourigault: Conceptualization (lead); formal analysis (lead); investigation (lead); methodology (lead); project administration (supporting); validation (supporting); writing – original draft (lead); writing – review and editing (lead). **Charly Dupont:** Formal analysis (supporting); investigation (supporting); writing – review and editing (supporting). **Jonas Desjardins:** Formal analysis (supporting); investigation (supporting); writing – review and editing (supporting). **Thierry Doan:** Conceptualization (lead); formal analysis (lead); investigation (supporting); project administration (supporting); supervision (lead); validation (lead); writing – review and editing (supporting). **Mathilde Bouteiller:** Investigation (supporting). **Hugo Le Guenno:** Investigation (supporting). **Sylvie Chevalier:** Resources (supporting); writing – review and editing (supporting). **Corinne Barbey:** Conceptualization (equal); funding acquisition (equal); methodology (equal); resources (equal); supervision (equal); validation (equal); writing – review and editing (supporting). **Xavier Latour:** Conceptualization (lead); formal analysis (supporting); funding acquisition (supporting); methodology (supporting); project administration (supporting); resources (supporting); supervision (lead); writing – review and editing (supporting). **Eric Cascales:** Conceptualization (lead); formal analysis (lead); funding acquisition (lead); investigation (supporting); methodology (supporting); project administration (lead); resources (lead); supervision (lead); validation (lead); visualization (supporting); writing – original draft (lead); writing – review and editing (equal). **Annabelle Merieau:** Conceptualization (lead); formal analysis (lead); funding acquisition (lead); investigation (supporting); project administration (lead); resources (lead); supervision (lead); validation (lead); writing – original draft (lead); writing – review and editing (supporting).

ACKNOWLEDGEMENTS

The authors thank Michaël Deghelt and Jean-François Collet (De Duve Institute, Brussels, Belgium) for kindly providing plasmid pTHV037dsbA-SP-msfTq2O_sol-Cytomcherry before publication, and Dukas Jurenas and Maïalène Chabalier for plasmid pBAD33tat. The authors thank members of the CBSA and Cascales laboratories for their discussions. This research was supported by grants from French institutions (Structure Fédérative de Recherche Normandie Végétal NORVEGE Fed4277, Ministère de l'Enseignement Supérieur, de la Recherche et de l'Innovation, Régions Bretagne, Normandie & Pays de Loire, the Evreux Portes de Normandie agglomeration and the Pôle de Compétitivité Valorial), FEDER (European Union), the CNRS, the Aix-Marseille Université and by grants from the Fondation pour la Recherche Médicale (FRM, DEQ20180339165) and the Fondation Bettencourt-Schueller to Eric Cascales. Jonas B. Desjardins thesis work is supported by a doctoral school fellowship from the FRM (ECO202206015565). The authors thank the Ecole Normande de Biologie Intégrative Santé et Environnement and the Société Française de Phytopathologie for kindly providing help for mobility.

CONFLICT OF INTEREST STATEMENT

The authors declare no conflicts of interest.

DATA AVAILABILITY STATEMENT

The data that support the findings of this study are available from the corresponding author upon reasonable request.

ORCID

Eric Cascales https://orcid.org/0000-0003-0611-9179

REFERENCES

Alcoforado Diniz, J., Liu, Y.-C. & Coulthurst, S.J. (2015) Molecular weaponry: diverse effectors delivered by the type VI secretion system. *Cellular Microbiology*, 17, 1742–1751. Available from: https://doi.org/10.1111/cmi.12532

Allsopp, L.P., Bernal, P., Nolan, L.M. & Filloux, A. (2020) Causalities of war: the connection between type VI secretion system and microbiota. *Cellular Microbiology*, 22, e13153. Available from: https://doi.org/10.1111/cmi.13153

Aschtgen, M.S., Bernard, C.S., Bentzmann, S., Lloubès, R. & Cascales, E. (2008) SciN is an outer membrane lipoprotein

required for type VI secretion in Enteroaggregative *Escherichia coli*. *Journal of Bacteriology*, 190, 7523–7531. Available from: https://doi.org/10.1128/JB.00945-08

Aschtgen, M.S., Gavioli, M., Dessen, A., Lloubès, R. & Cascales, E. (2010) The SciZ protein anchors the enteroaggregative *Escherichia coli* type VI secretion system to the cell wall. *Molecular Microbiology*, 75, 886–899. Available from: https://doi.org/10.1111/j.1365-2958.2009.07028.x

Barbey, C., Crépin, A., Bergeau, A., Ouchiha, A., Mijouin, L., Taupin, L. et al. (2013) In planta biocontrol of *Pectobacterium atrosepticum* by *Rhodococcus erythropolis* involves silencing of pathogen communication by the rhodococcal gamma-lactone catabolic pathway. *PLoS One*, 8, e66642. Available from: https://doi.org/10.1371/journal.pone.0066642

Barnard, A.M.L. & Salmond, G.P.C. (2007) Quorum sensing in *Erwinia* species. *Analytical and Bioanalytical Chemistry*, 387, 415–423. Available from: https://doi.org/10.1007/s00216-006-0701-1

Basler, M. (2015) Type VI secretion system: secretion by a contractile nanomachine. *Philosophical Transactions of the Royal Society B: Biological Sciences*, 370, 20150021. Available from: https://doi.org/10.1098/rstb.2015.0021

Basler, M., Pilhofer, M., Henderson, G.P., Jensen, G.J. & Mekalanos, J.J. (2012) Type VI secretion requires a dynamic contractile phage tail-like structure. *Nature*, 483, 182–186. Available from: https://doi.org/10.1038/nature10846

Bayer-Santos, E., Lima, L.D.P., Ceseti, L.M., Ratagami, C.Y., de Santana, E.S., da Silva, A.M. et al. (2018) *Xanthomonas citri* T6SS mediates resistance to *Dictyostelium* predation and is regulated by an ECF σ factor and cognate Ser/Thr kinase. *Environmental Microbiology*, 20, 1562–1575. Available from: https://doi.org/10.1111/1462-2920.14085

Bernal, P., Allsopp, L.P., Filloux, A. & Llamas, M.A. (2017) The *Pseudomonas putida* T6SS is a plant warden against phytopathogens. *The ISME Journal*, 11, 972–987. Available from: https://doi.org/10.1038/ismej.2016.169

Bernal, P., Llamas, M.A. & Filloux, A. (2018) Type VI secretion systems in plant-associated bacteria. *Environmental Microbiology*, 20, 1–15. Available from: https://doi.org/10.1111/1462-2920.13956

Bingle, L.E.H., Bailey, C.M. & Pallen, M.J. (2008) Type VI secretion: a beginner's guide. *Current Opinion in Microbiology*, 11, 3–8. Available from: https://doi.org/10.1016/j.mib.2008.01.006

Bogdanov, M. (2017) Mapping of membrane protein topology by substituted cysteine accessibility method (SCAMTM). In: Journet, L. & Cascales, E. (Eds.) *Bacterial protein secretion systems. Methods in molecular biology*, Vol. 1615. New York, NY: Springer New York, pp. 105–128. Available from: https://doi.org/10.1007/978-1-4939-7033-9_9

Bouteiller, M., Gallique, M., Bourigault, Y., Kosta, A., Hardouin, J., Massier, S. et al. (2020) Crosstalk between the type VI secretion system and the expression of class IV flagellar genes in the *Pseudomonas fluorescens* MFE01 strain. *Microorganisms*, 8, 622. Available from: https://doi.org/10.3390/microorganisms8050622

Boyer, F., Fichant, G., Berthod, J., Vandenbrouck, Y. & Attree, I. (2009) Dissecting the bacterial type VI secretion system by a genome wide in silico analysis: what can be learned from available microbial genomic resources? *BMC Genomics*, 10, 104. Available from: https://doi.org/10.1186/1471-2164-10-104

Brackmann, M., Nazarov, S., Wang, J. & Basler, M. (2017) Using force to punch holes: mechanics of contractile nanomachines. *Trends in Cell Biology*, 27, 623–632. Available from: https://doi.org/10.1016/j.tcb.2017.05.003

Brunet, Y.R., Espinosa, L., Harchouni, S., Mignot, T. & Cascales, E. (2013) Imaging type VI secretion-mediated bacterial killing. *Cell Reports*, 3, 36–41. Available from: https://doi.org/10.1016/j.celrep.2012.11.027

Cascales, E. (2008) The type VI secretion toolkit. *EMBO Reports*, 9, 735–741. Available from: https://doi.org/10.1038/embor.2008.131

Cassan, F.D., Coniglio, A., Amavizca, E., Maroniche, G., Cascales, E., Bashan, Y. et al. (2021) The *Azospirillum brasilense* type VI secretion system promotes cell aggregation, biocontrol protection against phytopathogens and attachment to the microalgae *Chlorella sorokiniana*. *Environmental Microbiology*, 23, 6257–6274. Available from: https://doi.org/10.1111/1462-2920.15749

Ceseti, L.M., Santana, E.S., Ratagami, C.Y., Barreiros, Y., Lima, L.P., Dunger, G. et al. (2019) The *Xanthomonas citri Pv. citri* type VI secretion system is induced during epiphytic colonization of Citrus. *Current Microbiology*, 76, 1105–1111. Available from: https://doi.org/10.1007/s00284-019-01735-3

Chane, A., Barbey, C., Robert, M., Merieau, A., Ghiorghi, Y.K., Cirou, A.B. et al. (2019) Biocontrol of soft rot: confocal microscopy highlights virulent pectobacterial communication and its jamming by rhodococcal quorum-quenching. *Molecular Plant-Microbe Interactions*, 32, 802–812. Available from: https://doi.org/10.1094/MPMI-11-18-0314-R

Chassaing, B. & Cascales, E. (2018) Antibacterial weapons: targeted destruction in the microbiota. *Trends in Microbiology*, 26, 329–338. Available from: https://doi.org/10.1016/j.tim.2018.01.006

Chen, C., Yang, X. & Shen, X. (2019) Confirmed and potential roles of cacterial T6SSs in the intestinal ecosystem. *Frontiers in Microbiology*, 10, 1484. Available from: https://doi.org/10.3389/fmicb.2019.01484

Cherrak, Y., Flaugnatti, N., Durand, E., Journet, L. & Cascales, E. (2019) Structure and activity of the type VI secretion system. *Microbiology Spectrum*, 7, PSIB0031-2019. Available from: https://doi.org/10.1128/microbiospec.PSIB-0031-2019

Chou, S., Bui, N.K., Russell, A.B., Lexa, K.W., Gardiner, T.E., LeRoux, M. et al. (2012) Structure of a peptidoglycan amidase effector targeted to Gram-negative bacteria by the type VI secretion system. *Cell Reports*, 1, 656–664. Available from: https://doi.org/10.1016/j.celrep.2012.05.016

Cianfanelli, F.R., Monlezun, L. & Coulthurst, S.J. (2016) Aim, load, fire: the type VI secretion system, a bacterial nanoweapon. *Trends in Microbiology*, 24, 51–62. Available from: https://doi.org/10.1016/j.tim.2015.10.005

Coulthurst, S.J. (2019) The type VI secretion system: a versatile bacterial weapon. *Microbiology*, 165, 503–515. Available from: https://doi.org/10.1099/mic.0.000789

Crépin, A., Cirou, A.B., Barbey, B., Farmer, C., Hélias, V., Burini, J.F. et al. (2012) *N*-acyl homoserine lactones in diverse *Pectobacterium* and *Dickeya* plant pathogens: diversity, abundance, and involvement in virulence. *Sensors*, 12, 3484–3497. Available from: https://doi.org/10.3390/s120303484

Davey, M.E., Caiazza, N.C. & O'Toole, G.A. (2003) Rhamnolipid surfactant production affects biofilm architecture in *Pseudomonas aeruginosa* PAO1. *Journal of Bacteriology*, 185, 1027–1036. Available from: https://doi.org/10.1128/JB.185.3.1027-1036.2003

Decoin, V., Barbey, C., Bergeau, D., Latour, X., Feuilloley, M.G.J., Orange, N. et al. (2014) A type VI secretion system is involved in *Pseudomonas fluorescens* bacterial competition. *PLoS One*, 9, e89411. Available from: https://doi.org/10.1371/journal.pone.0089411

Decoin, V., Gallique, M., Barbey, C., Le Mauff, F., Duclairoir Poc, C., Feuilloley, M.G.J. et al. (2015) A *Pseudomonas fluorescens* type 6 secretion system is related to mucoidy, motility and bacterial competition. *BMC Microbiology*, 15, 72. Available from: https://doi.org/10.1186/s12866-015-0405-9

Deghelt, M., Cho, S.-H., Govers, S.K., Janssens, A., Dachsbeck, A., Remaut, H.K. et al. (2023) The outer membrane and peptidoglycan layer form a single mechanical device balancing turgor.

BioRxiv. Available from: https://doi.org/10.1101/2023.04.29.538579

Diallo, S., Crépin, A., Barbey, C., Orange, N., Burini, J.F. & Latour, X. (2011) Mechanisms and recent advances in biological control mediated through the potato rhizosphere. *FEMS Microbiology Ecology*, 75, 351–364. Available from: 10.1111/j.1574-6941.2010.01023.x

Dupuis, B., Nkuriyingoma, P. & Van Gijsegem, F. (2021) Economic impact of *Pectobacterium* and *Dickeya* species on potato crops: a review and case study. In: Van Gijsegem, F., van der Wolf, J.-M. & Toth, I.K. (Eds.) *Plant diseases caused by Dickeya and Pectobacterium species*. Springer Nature. Available from: https://doi.org/10.1007/978-3-030-61459-1_8

Durán, D., Bernal, P., Vazquez-Arias, D., Blanco-Romero, E., Garrido-Sanz, D., Redondo-Nieto, M. et al. (2021) *Pseudomonas fluorescens* F113 type VI secretion systems mediate bacterial killing and adaption to the rhizosphere microbiome. *Scientific Reports*, 11, 5772. Available from: https://doi.org/10.1038/s41598-021-85218-1

Durand, E., Cambillau, C., Cascales, E. & Journet, L. (2014) VgrG, Tae, Tle, and beyond: the versatile arsenal of type VI secretion effectors. *Trends in Microbiology*, 22, 498–507. Available from: https://doi.org/10.1016/j.tim.2014.06.004

El-Sayed, A.K., Hothersall, J. & Thomas, C.M. (2001) Quorum-sensing-dependent regulation of biosynthesis of the polyketide antibiotic mupirocin in *Pseudomonas fluorescens* NCIMB 10586. *Microbiology*, 147, 2127–2139.

Filip, C., Fletcher, G., Wulff, J.L. & Earhart, C.F. (1973) Solubilization of the cytoplasmic membrane of *Escherichia coli* by the ionic detergent sodium-lauryl sarcosinate. *Journal of Bacteriology*, 115, 717–722. Available from: https://doi.org/10.1128/jb.115.3.717-722.1973

Fu, Y., Waldor, M.K. & Mekalanos, J.J. (2013) Tn-Seq analysis of *vibrio cholerae* intestinal colonization reveals a role for T6SS-mediated antibacterial activity in the host. *Cell Host & Microbe*, 14, 652–663. Available from: https://doi.org/10.1016/j.chom.2013.11.001

Gallegos-Monterrosa, R. & Coulthurst, S.J. (2021) The ecological impact of a bacterial weapon: microbial interactions and the type VI secretion system. *FEMS Microbiology Reviews*, 45, fuab033. Available from: https://doi.org/10.1093/femsre/fuab033

Gallique, M., Bouteiller, M. & Merieau, A. (2017) The type VI secretion system: a dynamic system for bacterial communication? *Frontiers in Microbiology*, 8, 1454. Available from: https://doi.org/10.3389/fmicb.2017.01454

Gallique, M., Decoin, V., Barbey, C., Rosay, T., Feuilloley, M.G.J., Orange, O. et al. (2017) Contribution of the *Pseudomonas fluorescens* MFE01 type VI secretion system to biofilm formation. *PLoS One*, 12, e0170770. Available from: https://doi.org/10.1371/journal.pone.0170770

Gerc, A.J., Diepold, A., Trunk, A., Porter, M., Rickman, C., Armitage, J.P. et al. (2015) Visualization of the *Serratia* type VI secretion system reveals unprovoked attacks and dynamic assembly. *Cell Reports*, 12, 2131–2142. Available from: https://doi.org/10.1016/j.celrep.2015.08.053

Haas, D. & Défago, G. (2005) Biological control of soil-borne pathogens by fluorescent pseudomonads. *Nature Reviews Microbiology*, 3, 307–319. Available from: https://doi.org/10.1038/nrmicro1129

Hernandez, R.E., Gallegos-Monterrosa, R. & Coulthurst, S.J. (2020) Type VI secretion system effector proteins: effective weapons for bacterial competitiveness. *Cellular Microbiology*, 22, e13241. Available from: https://doi.org/10.1111/cmi.13241

Ho, B.T., Dong, T.G. & Mekalanos, J.J. (2014) A view to a kill: the bacterial type VI secretion system. *Cell Host & Microbe*, 15, 9–21. Available from: https://doi.org/10.1016/j.chom.2013.11.008

Jurenas, D. & Journet, L. (2021) Activity, delivery, and diversity of type VI secretion effectors. *Molecular Microbiology*, 115, 383–394. Available from: https://doi.org/10.1111/mmi.14648

Kapitein, N. & Mogk, A. (2013) Deadly syringes: type VI secretion system activities in pathogenicity and interbacterial competition. *Current Opinion in Microbiology*, 16, 52–58. Available from: https://doi.org/10.1016/j.mib.2012.11.009

Lin, J., Zhang, W., Cheng, J., Yang, X., Zhu, K., Wang, Y. et al. (2017) A *Pseudomonas* T6SS effector recruits PQS-containing outer membrane vesicles for iron acquisition. *Nature Communications*, 8, 14888. Available from: https://doi.org/10.1038/ncomms14888

Liu, H., Coulthurst, S.J., Pritchard, L., Hedley, P.E., Ravensdale, M., Humphris, S. et al. (2008) Quorum sensing coordinates brute force and stealth modes of infection in the plant pathogen *Pectobacterium atrosepticum*. *PLoS Pathogens*, 4, e1000093. Available from: https://doi.org/10.1371/journal.ppat.1000093

Ma, L.S., Hachani, A., Lin, J.S., Filloux, A. & Lai, E.M. (2014) *Agrobacterium tumefaciens* deploys a superfamily of type VI secretion DNase effectors as weapons for interbacterial competition in planta. *Cell Host & Microbe*, 16, 94–104. Available from: https://doi.org/10.1016/j.chom.2014.06.002

Mansfield, J., Genin, S., Magori, S., Citovsky, V., Sriariyanum, M., Ronald, P. et al. (2012) Top 10 plant pathogenic bacteria in molecular plant pathology. *Molecular Plant Pathology*, 13, 614–629. Available from: https://doi.org/10.1111/j.1364-3703.2012.00804.x

Marchi, M., Boutin, M., Gazengel, K., Rispe, C., Gauthier, J.P., Guillerm-Erckelboudt, A.Y. et al. (2013) Genomic analysis of the biocontrol strain *Pseudomonas fluorescens* Pf29Arp with evidence of T3SS and T6SS gene expression on plant roots. *Environmental Microbiology Reports*, 5, 393–403. Available from: https://doi.org/10.1111/1758-2229.12048

Maurhofer, M., Reimmann, C., Schmidli-Sacherer, P., Heeb, S., Haas, D. & Défago, G. (1998) Salicylic acid biosynthetic genes expressed in *Pseudomonas fluorescens* strain P3 improve the induction of systemic resistance in tobacco against tobacco necrosis virus. *Phytopathology*, 88, 678–684. Available from: https://doi.org/10.1094/PHYTO.1998.88.7.678

Miller, J.F. (2013) Gaming the competition in microbial cell-cell interactions. *EMBO Journal*, 32, 778–780. Available from: https://doi.org/10.1038/emboj.2013.45

Murdoch, S.L., Trunk, K., English, G., Fritsch, M.J., Pourkarimi, E. & Coulthurst, S.J. (2011) The opportunistic pathogen *Serratia marcescens* utilizes type VI secretion to target bacterial competitors. *Journal of Bacteriology*, 193, 6057–6069. Available from: https://doi.org/10.1128/JB.05671-11

Newman, J.R. & Fuqua, C. (1999) Broad-host-range expression vectors that carry the L-arabinose-inducible Escherichia coli araBAD promoter and the araC regulator. *Gene*, 227, 197–203. Available from: https://doi.org/10.1016/s0378-1119(98)00601-5

Ostrowski, A., Cianfanelli, F.R., Porter, M., Mariano, G., Peltier, J., Wong, J.J. et al. (2018) Killing with proficiency: integrated post-translational regulation of an offensive type VI secretion system. *PLoS Pathogens*, 14, e1007230. Available from: https://doi.org/10.1371/journal.ppat.1007230

Pérombelon, M.C.M. (2002) Potato diseases caused by soft rot Erwinias: an overview of pathogenesis. *Plant Pathology*, 51, 1–12. Available from: https://doi.org/10.1046/j.0032-0862.2001

Radkov, A., Sapiro, A.L., Flores, S., Henderson, C., Saunders, H., Kim, R. et al. (2022) Antibacterial potency of type VI amidase effector toxins is dependent on substrate topology and cellular context. *eLife*, 11, e79796. Available from: https://doi.org/10.7554/eLife.79796

Russell, A.B., Hood, R.D., Bui, N.K., LeRoux, M., Vollmer, W. & Mougous, J.D. (2011) Type VI secretion delivers bacteriolytic effectors to target cells. *Nature*, 475, 343–347. Available from: https://doi.org/10.1038/nature10244

Russell, A.B., Peterson, S.B. & Mougous, J.D. (2014) Type VI secretion system effectors: poisons with a purpose. *Nature Reviews Microbiology*, 12, 137–148. Available from: https://doi.org/10.1038/nrmicro3185

Russell, A.B., Singh, P., Brittnacher, M., Bui, N.K., Hood, R.D., Carl, M.A. et al. (2012) A widespread bacterial type VI secretion effector superfamily identified using a heuristic approach. *Cell Host & Microbe*, 11, 538–549. Available from: https://doi.org/10.1016/j.chom.2012.04.007

Sana, T.G., Flaugnatti, N., Lugo, K.A., Lam, L.H., Jacobson, A., Baylot, V. et al. (2016) *Salmonella* Typhimurium utilizes a T6SS-mediated antibacterial weapon to establish in the host gut. *Proceedings of the National Academy of Sciences of the United States of America*, 113, E5044–E5051. Available from: https://doi.org/10.1073/pnas.1608858113

Santin, Y.G., Doan, T., Journet, L. & Cascales, E. (2019) Cell width dictates type VI secretion tail length. *Current Biology*, 29, 3707–3713.e3. Available from: https://doi.org/10.1016/j.cub.2019.08.058

Santin, Y.G., Doan, T., Lebrun, R., Espinosa, L., Journet, L. & Cascales, E. (2018) In vivo TssA proximity labelling during type VI secretion biogenesis reveals TagA as a protein that stops and holds the sheath. *Nature Microbiology*, 3, 1304–1313. Available from: https://doi.org/10.1038/s41564-018-0234-3

Schneider, C.A., Rasband, W.S. & Eliceiri, K.W. (2012) NIH image to ImageJ: 25 years of image analysis. *Nature Methods*, 9, 671–675. Available from: https://doi.org/10.1038/nmeth.2089

Schneider, J.P., Nazarov, S., Adaixo, R., Liuzzo, M., Ringel, P.D., Stahlberg, H. et al. (2019) Diverse roles of TssA-like proteins in the assembly of bacterial type VI secretion systems. *The EMBO Journal*, 38, e100825. Available from: https://doi.org/10.15252/embj.2018100825

Simon, R., Priefer, U. & Pühler, A. (1983) A broad host range mobilization system for in vivo genetic engineering: transposon mutagenesis in gram negative bacteria. *Nature Biotechnology*, 1, 784–791.

Smadja, B., Latour, X., Faure, D., Chevalier, S., Dessaux, Y. & Orange, N. (2004) Involvement of N-acylhomoserine lactones throughout plant infection by *Erwinia carotovora subsp. atroseptica* (*Pectobacterium atrosepticum*). *Molecular Plant-Microbe Interactions*, 17, 1269–1278. Available from: https://doi.org/10.1094/MPMI.2004.17.11.1269

Taylor, N.M.I., van Raaij, M.J. & Leiman, P.G. (2018) Contractile injection systems of bacteriophages and related systems. *Molecular Microbiology*, 108, 6–15. Available from: https://doi.org/10.1111/mmi.13921

Tian, Y., Zhao, Y., Wu, X., Liu, F., Hu, B. & Walcott, R.R. (2015) The type VI protein secretion system contributes to biofilm formation and seed-to-seedling transmission of *Acidovorax citrulli* on melon. *Molecular Plant Pathology*, 16, 38–47. Available from: https://doi.org/10.1111/mpp.12159

Toth, I.K., Barny, M.A., Brurberg, M.B., Condemine, G., Czajkowski, R., Elphinstone, J.G. et al. (2021) *Pectobacterium* and *Dickeya*: environment to disease development. In: Van Gijsegem, F., van der Wolf, J.M. & Toth, I.K. (Eds.) *Plant diseases caused by Dickeya and Pectobacterium species*. Springer Nature. Available from: https://doi.org/10.1007/978-3-030-61459-1_3

Turner, T.R., James, E.K. & Poole, P.S. (2013) The plant microbiome. *Genome Biology*, 14, 209. Available from: https://doi.org/10.1186/gb-2013-14-6-209

Vacheron, J., Péchy-Tarr, M., Brochet, S., Heiman, C.M., Stojiljkovic, M., Maurhofer, M. et al. (2019) T6SS contributes to gut microbiome invasion and killing of an herbivorous pest insect by plant-beneficial *Pseudomonas protegens*. *The ISME Journal*, 13, 1318–1329. Available from: https://doi.org/10.1038/s41396-019-0353-8

van der Ent, F. & Löwe, J. (2006) RF cloning: a restriction-free method for inserting target genes into plasmids. *Journal of Biochemical and Biophysical Methods*, 67, 67–74. Available from: https://doi.org/10.1016/j.jbbm.2005.12.008

Van Gijsegem, F., Hugouvieux-Cotte-Pattat, N., Kraepiel, Y., Lojkowska, E., Moleleki, L.N., Gorshkov, V. et al. (2021) Molecular interactions of *Pectobacterium* and *Dickeya* with plants. In: Van Gijsegem, F., van der Wolf, J.M. & Toth, I.K. (Eds.) *Plant diseases caused by Dickeya and Pectobacterium species*. Springer Nature. Available from: https://doi.org/10.1007/978-3-030-61459-1_4

Wang, J., Brodmann, M. & Basler, M. (2019) Assembly and subcellular localization of bacterial type VI secretion systems. *Annual Review of Microbiology*, 73, 621–638. Available from: https://doi.org/10.1146/annurev-micro-020518-115420

Wang, T., Hu, Z., Du, X., Shi, Y., Dang, J., Lee, M. et al. (2020) A type VI secretion system delivers a cell wall amidase to target bacterial competitors. *Molecular Microbiology*, 114, 308–321. Available from: https://doi.org/10.1111/mmi.14513

Whitney, J.C., Chou, S., Russell, A.B., Biboy, J., Gardiner, T.E., Ferrin, M.A. et al. (2013) Identification, structure, and function of a novel type VI secretion peptidoglycan glycoside hydrolase effector-immunity pair. *Journal of Biological Chemistry*, 288, 26616–26624. Available from: https://doi.org/10.1074/jbc.M113.488320

Yang, X., Liu, H., Zhang, Y. & Shen, X. (2021) Roles of type VI secretion system in transport of metal ions. *Frontiers in Microbiology*, 12, 756136. Available from: https://doi.org/10.3389/fmicb.2021.756136

Zhang, L., Xu, J., Xu, J., Chen, K., He, L. & Feng, J. (2012) TssM is essential for virulence and required for type VI secretion in *Ralstonia solanacearum*. *Journal of Plant Diseases and Protection*, 119, 125–134. Available from: https://doi.org/10.1007/BF03356431

SUPPORTING INFORMATION

Additional supporting information can be found online in the Supporting Information section at the end of this article.

How to cite this article: Bourigault, Y., Dupont, C.A., Desjardins, J.B., Doan, T., Bouteiller, M., Le Guenno, H. et al. (2023) *Pseudomonas fluorescens* MFE01 delivers a putative type VI secretion amidase that confers biocontrol against the soft-rot pathogen *Pectobacterium atrosepticum*. *Environmental Microbiology*, 1–16. Available from: https://doi.org/10.1111/1462-2920.16492

Supplemental Information

Pseudomonas fluorescens MFE01 delivers a putative type VI secretion amidase that confers biocontrol against the soft-rot pathogen *Pectrobacterium atrosepticum.*

Yvann Bourigault, Charly Dupont, Jonas B. Desjardins, Thierry Doan, Mathilde Bouteiller, Hugo Le Guenno, Sylvie Chevalier, Corinne Barbey, Xavier Latour, Eric Cascales, and Annabelle Merieau

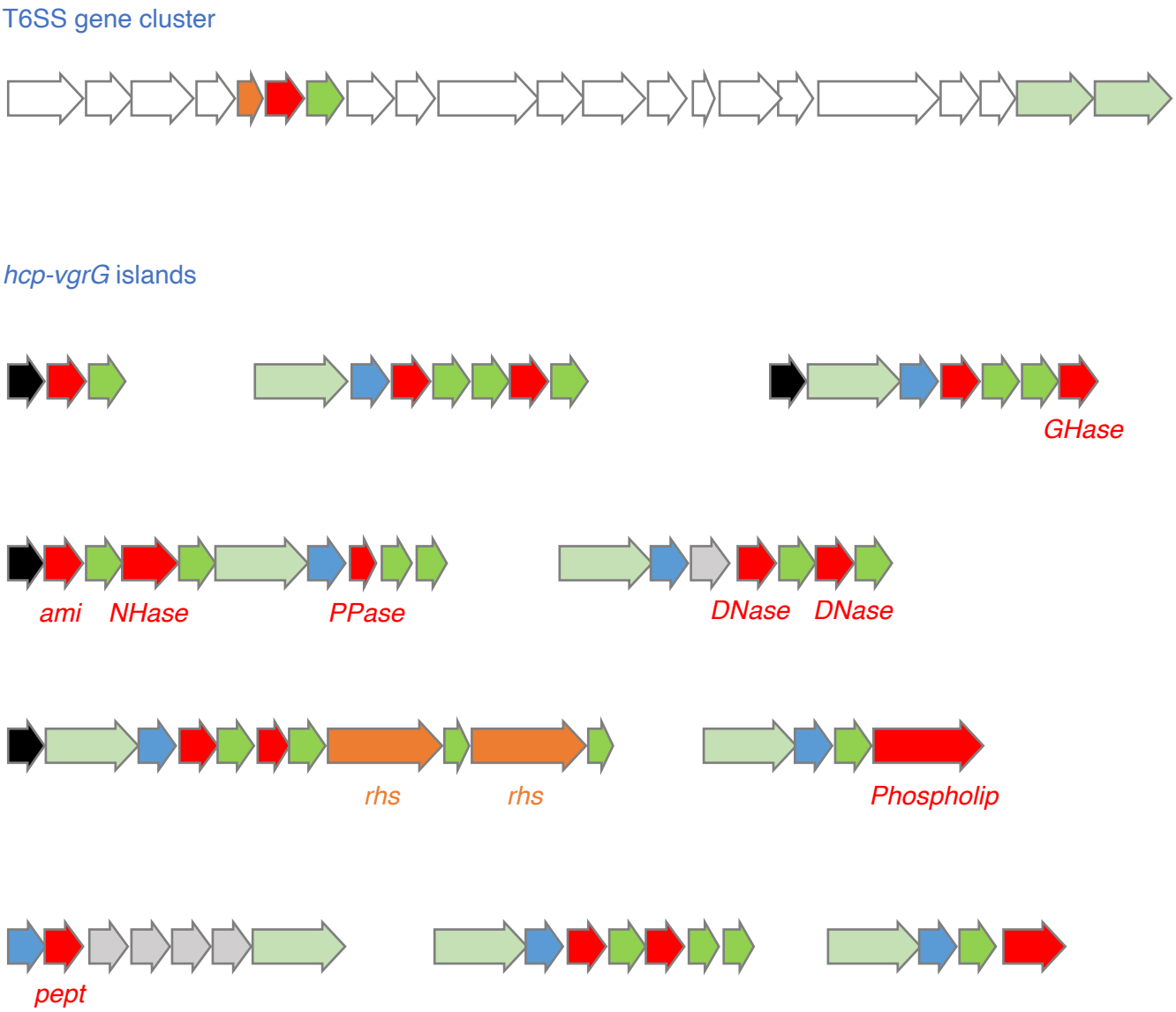

Supplemental Figure S1. Schematic representation of the *P. fluorescens* MFE01 T6SS gene cluster and *hcp*, *vgrG* and *hcp-vgrG* islands. The T6SS gene cluster and the *hcp*, *vgrG* and *hcp-vgrG* islands scattered on the MFE01 genome are represented. The *hcp*, *vgrG* and *PAAR/rhs* genes are colored in black, light green and orange respectively. Putative effectors and immunities are colored in red and green, while potential adaptors or chaperones are colored in blue. When a function can be clearly inferred from the sequence of the potential effector, it is indicated (ami, amidase; NHase, Nudix hydrolase; PPase, pyrophosphatase; GHase, glycosylhydrolase; DNase, deoxynuclease; Phospholip, phospholipase; pept, peptidase).

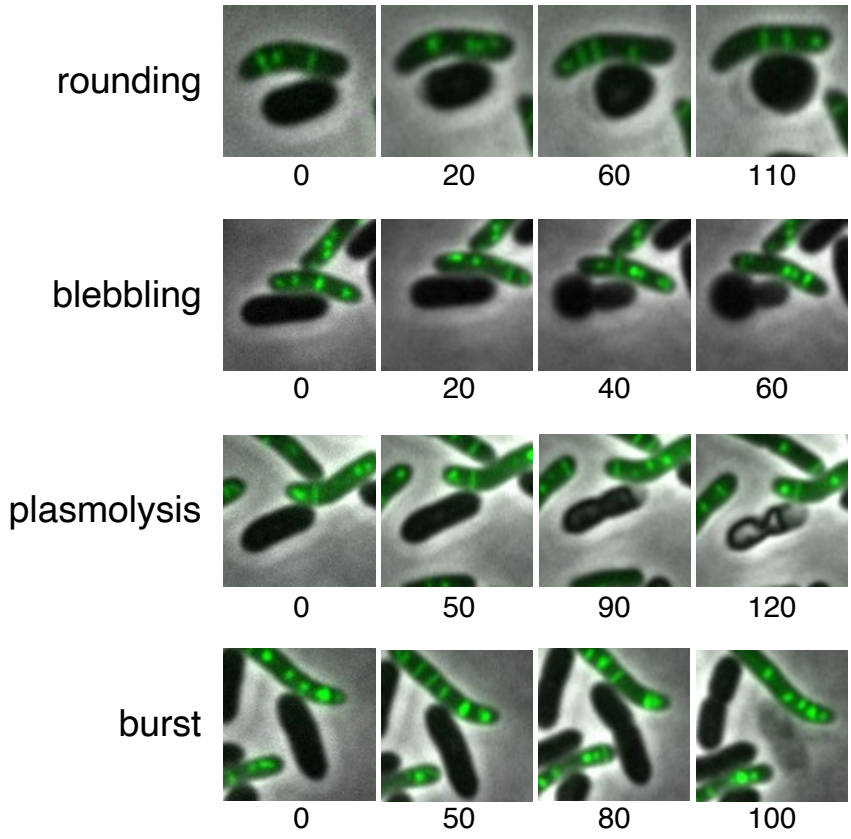

Supplemental Figure S2. Pca cell damages observed after incubation with MFE01. Time-lapse fluorescence recordings highlighting the different morphologic changes of Pca observed when co-cultured with MFE01 TssB-sfGFP (time in min).

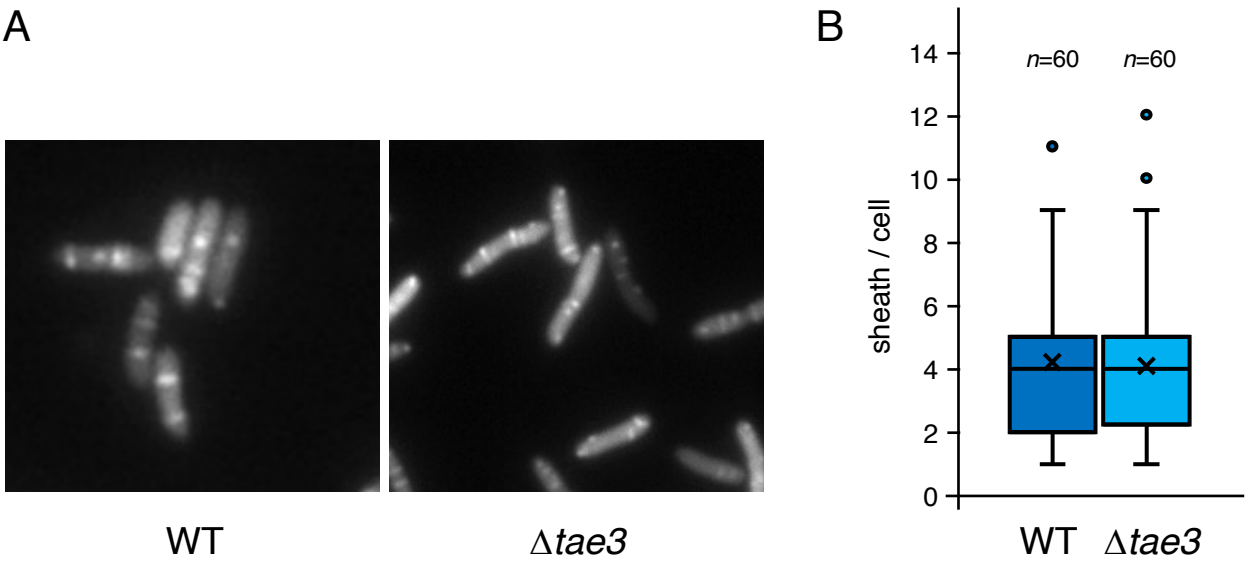

Supplemental Figure S3. Deletion of *tae3* does not impact sheath assembly. (**A**) Representative fluorescence microscopy field of MFE01 wild-type and its isogenic Δ*tae3* mutant producing TssB-sfGFP. (**B**) Statistical analyses. Box plot representations of the number of T6SS sheath per cell The internal horizontal line and cross represent the median and mean values, respectively; the boundaries of the internal box plot correspond to the 25th and 75th percentiles; whiskers correspond to the 10^{th} and 90^{th} percentiles. Outliers are shown as closed circles. The number of analysed events (*n*) is indicated on top of each graph.

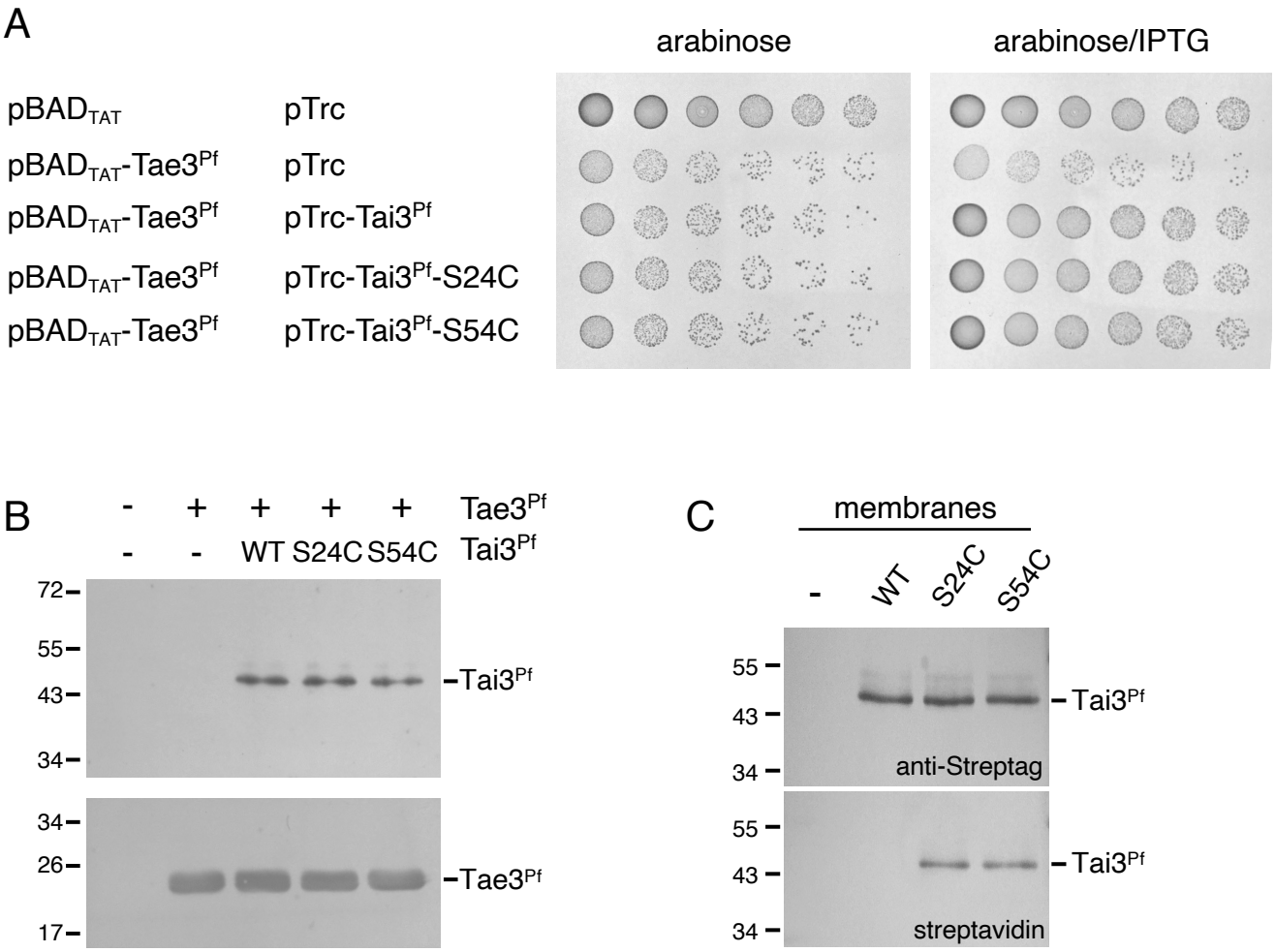

Supplemental Figure S4. The Tai3^{Pf} S24C and S54C variants are functional and accessible to MPB. (**A**) Toxicity and rescue assays in the heterologous host *E. coli*. Cultures of *E. coli* cells bearing the empty or *tae3*-encoded pBAD33tat plasmid and the empty or wild-type or mutant *tai3*-encoded pTrc99A plasmid were serially diluted and 10^{-1} to 10^{-6} dilutions (from left to right) were spotted on LB-agar plates supplemented with 0.2 % L-arabinose to induce expression of *tae3*, or supplemented with 0.2% of L-arabinose and 0.5 mM of IPTG to induce expression of *tae3* and *tai3*, respectively. (**B**) Western-blot analyses of *E. coli* cells producing Tae3^{Pf} and Tai3^{Pf}. Cell extracts of *E. coli cells* producing Tae3^{Pf} and wild-type (WT) or S24C/S54C mutants of Tai3^{Pf} were analysed by SDS-PAGE, transferred onto nitrocellulose, and immunodetected with anti-StrepTag (Tai3^{Pf}, upper panel) or anti-VSV-G (Tae3^{Pf}, lower panel) monoclonal antibodies. Molecular weight markers are indicated on the left. (**C**) Substituted Cysteine Accessibility Method. Whole membranes of *E. coli* cells producing Strep-tagged wild-type (WT) or S24C or S54C Tai3^{Pf} were treated with MPB to label accessible thiol groups. After Tai3^{Pf} precipitation, the samples were analysed by SDS-PAGE, transferred onto nitrocellulose, and immunodetected with anti-StrepTag monoclonal antibody (upper panel) and streptavidin coupled to alkaline phosphatase (lower panel). Molecular weight markers are indicated on the left.

Supplemental Table S1. Strains and Plasmids used in this study

Strain or plasmid	Relevant characteristics	Reference
Strain		
Pectobacterium atrosepticum CFBP6276	Potato soft rot pathogen	Smadja et al., 2003
Pseudomonas fluorescens MFE01 WT	Air isolate, Rif^R	Decoin et al., 2014
Pseudomonas fluorescens MFE01 Δ*tssC*	MFE01 with disruption of the *tssC* gene	Decoin et al., 2015
Pseudomonas fluorescens MFE01 Δ*tssC-R*	MFE01Δ*tssC* carrying a chromosomal copy of wild-type *tssC* re-introduced at the native locus.	Bouteiller et al., 2020
Pseudomonas fluorescens MFE01 *tssB*-sfGFP	MFE01 with translational fusion of sfGFP to *tssB*	This study
Pseudomonas fluorescens MFE01 Δ*tae3*	MFE01 with disruption of the *tae3* gene.	This study
Escherichia coli DH5α	Laboratory *E. coli* strain	NEB
Escherichia coli S17-1	*recA*. RP4	Simon et al., 1983
Plasmid		
pME6000	Replicative plasmid in *P. atrosepticum*, Tc^R	Maurhofer et al., 1998
pSMC2.1-*gfp*	Replicative plasmid in Gram-negative bacteria, Km^R, *gfp*	Davey et al., 2003
pAKE604	Conjugative suicide vector, Km^R, *sacB*	El-Sayed et al., 2001
pAKE604-*tssB*-sfGFP	pAKE604 containing '*tssA-tssB-sfGFP-tssC*' for chromosomal insertion of tssB-sfGFP at the native locus, Km^R, *sacB*	This study
pJN105	Replicative plasmid in *P. fluorescens.* pBBR1MCS-5 vector with P*araBAD* promoter, *araC*, Gm^R.	Newman and Fuqua, 1999
pJN105-Tae3	pJN105 vector expressing $Tae3^{Pf}$	This study
pTHV037dsbA-SP-msfTq20X-solcytomcherry	pTHV037 vector producing sfTq20 fused to the DsbA signal sequence (periplasm) and mCherry (cytoplasm)	Deghelt et al., 2023
pBAD33rbs	P*araBAD* promoter. RBS, Cm^R. P15A origin	M. Chabalier and D. Jurenas
pBAD-$Tae3^{Pf}$	pBAD33rbs expressing VSV-G-tagged $Tae3^{Pf}$.	This study

pBAD33tat	pBAD33 vector with RBS and TorA Tat signal sequence, P*araBAD* promoter. Cm^R. P15A origin	M. Chabalier and D. Jurenas
pBAD33tat-$Tae3^{Pf}$	pBAD33tat expressing VSV-G-tagged $Tae3^{Pf}$.	This study
pBAD33tat-$Tae3^{Pf}$-C18A	pBAD33tat expressing VSV-G-tagged $Tae3^{Pf}$ C18A variant.	This study
pBAD33tat-$Tae3^{Pf}$-H141A	pBAD33tat expressing VSV-G-tagged $Tae3^{Pf}$ H141A variant.	This study
pTrc99a	Cloning vector. P*trc-lac* promoter. Amp^R. ColE1 promoter.	Pharmacia
pTrc-$Tai3^{Pf}$	pTrc99a expressing Streptagged $Tai3^{Pf}$.	This study
pTrc-$Tai3^{Pf}$-S24C	pTrc99a expressing Streptagged $Tai3^{Pf}$ S24C variant.	This study
pTrc-$Tai3^{Pf}$-S54C	pTrc99a expressing Streptagged $Tai3^{Pf}$ S54C variant.	This study

Supplemental Table S2. Oligonucleotides used in this study.

Primer name	**Primer sequence (5'-3')**[a,b,c]
Muta1AmidaseHcp3-F	GATCCGCTTTATCGAATTGT
Muta2AmidaseHcp3-R	ATACTTCGTGGGTCCAGGTGAGTCGGTCATGCTCAGTTC
Muta3AmidaseHcp3-F	TCACCTGGACCCACGAAGTATGGCATTGCACATCTGTTTA
Muta4AmidaseHcp3-R	TCTTGTTGTCGAAGTTGAAG
YB58 (Chrs)	TAATAAGGATCCGATCGCTGCCAACGTCATG
YB59 (Chrs)	TAATAATCTAGACCCATGCTTTCGAAGTGG
YB51 (Plasmid)	CCGCAAGGAGAAAAGCCATG
YB52 (Plasmid)	TTATTTGTAGAGCTCATCCATG
F-Tae3-pJN	TAATAAGAATTCGACTTCGGTGAGGCTGGTCCGTGAA
R-Tae3-pJN	TAATAATCTAGATTCGACCACAACCATACAAC
5-pBADrbs-$Tae3^{Pf}$	GGGATCCTCTAGAAGGAGGGTCGACTGATGGTGAGGCTGGTCCGTGAACTGAGC
3-pBADrbs-$Tae3^{Pf}$	GCCAAGCTTGCATGCCTGCAGGATTTA*TTTTCCTAATCTATTCATTTCAATATCTGTATA*GACGTTGAAGATGCGCAGCGAAAGC
5-pBADtat-$Tae3^{Pf}$	GCCGCGACGTGCGACTGCGGCGGTGAGGCTGGTCCGTGAACTGAGC
3-pBADtat-$Tae3^{Pf}$	GCTTGCATGCCTGCAGGACTGTCGACTTA*TTTTCCTAATCTATTCATTTCAATATCTGTATA*GACGTTGAAGATGCGCAGCGAAAGC

5-pTrc-Tai3^{Pf}	GGATAACAATTTCACACAGGAAACAGACCATG*TGGAGCCAT CCGCAGTTTGAAAAAAGCGCT*CTGGACTGGAAAAACCGCGCG G
3-pTrc-Tai3^{Pf}	CCCGGGTACCGAGCTCGAATTCTCAGCCCTGATTGAGCAGTT GACGC
A-Tae3-C18A	CCACGAGCGCCAGCATGTC**GCT**GGCGTGGAGGAGGCGCTGG CG
B-Tae3-C18A	CGCCAGCGCCTCCTCCACGCC**AGC**GACATGCTGGCGCTCGT GG
A-Tae3-H141A	CTGACGCCCAAGGCATTGCA**GCT**CTGTTTACCGACGACCAA GTG
B-Tae3-H14A	CACTTGGTCGTCGGTAAACAG**AGC**TGCAATGCCTTGGGCGT CAG
A-Tai3-S24A	GCCCAAGTCGGCCACCCGC**TGC**TATGTCGGCGGGCTGCTG
B-Tai3-S24A	CAGCAGCCCGCCGACATA**GCA**GCGGGTGGCCGACTTGGGC
A-Tai3-S54A	GCGCTGGGCTGGTACTGG**TGC**CAGGAACCGGAGCTGTTTC
B-Tai3-S54A	GAAACAGCTCCGGTTCCTG**GCA**CCAGTACCAGCCCAGCGC

[a] restriction site or sequence annealing on the target vector underlined
[b] tag sequence in *italics*
[c] mutagenized codon in **bold**